

# Modelling the influence of data structure on learning in neural networks: the Hidden Manifold Model

Sebastian Goldt,<sup>1,\*</sup> Marc Mézard,<sup>2,†</sup> Florent Krzakala,<sup>2,‡</sup> and Lenka Zdeborová<sup>1,§</sup>

<sup>1</sup>*Institut de Physique Théorique, CNRS, CEA, Université Paris-Saclay, France*

<sup>2</sup>*Laboratoire de Physique de l'École Normale Supérieure, Université PSL, CNRS,  
Sorbonne Université, Université Paris-Diderot, Sorbonne Paris Cité, Paris, France*

(Dated: May 5, 2020)

Understanding the reasons for the success of deep neural networks trained using stochastic gradient-based methods is a key open problem for the nascent theory of deep learning. The types of data where these networks are most successful, such as images or sequences of speech, are characterised by intricate correlations. Yet, most theoretical work on neural networks does not explicitly model training data, or assumes that elements of each data sample are drawn independently from some factorised probability distribution. These approaches are thus by construction blind to the correlation structure of real-world data sets and their impact on learning in neural networks. Here, we introduce a generative model for *structured* data sets that we call the *hidden manifold model* (HMM). The idea is to construct high-dimensional inputs that lie on a lower-dimensional manifold, with labels that depend only on their position within this manifold, akin to a single layer decoder or generator in a generative adversarial network. We demonstrate that learning of the hidden manifold model is amenable to an analytical treatment by proving a “Gaussian Equivalence Property” (GEP), and we use the GEP to show how the dynamics of two-layer neural networks trained using one-pass stochastic gradient descent is captured by a set of integro-differential equations that track the performance of the network at all times. This permits us to analyse in detail how a neural network learns functions of increasing complexity during training, how its performance depends on its size and how it is impacted by parameters such as the learning rate or the dimension of the hidden manifold.

## I. INTRODUCTION

The data sets on which modern neural networks are most successful, such as images [1, 2] or natural language [3], are characterised by complicated correlations. Yet, most theoretical works on neural networks in statistics or theoretical computer science do not model the structure of the training data at all [4, 5], which amounts to assuming that the data set is chosen in a worst-case (adversarial) manner. A line of theoretical works complementary to the statistics approach emanated from statistical physics [6–9]. These works model inputs as element-wise i.i.d. draws from some probability distribution, with labels that are either random or given by some random, but fixed function of the inputs. Despite providing valuable insights, these approaches are by construction blind to even basic statistical properties of real-world data sets such as their covariance structure. This lack of mathematical models for data sets is a major impediment for understanding the effectiveness of deep neural networks.

The structure present in realistic data sets can be illustrated well with classic data sets for image classification, such as the handwritten digits of MNIST [10] or the images of CIFAR10 [11]. The inputs that the neural network has to classify are images, so *a priori* the input

space is the high-dimensional  $\mathbb{R}^N$ , corresponding to the number of pixels, with  $N$  large. However, the inputs that can be recognised as actual images rather than random noise, span but a lower-dimensional manifold within  $\mathbb{R}^N$ , see Fig. 1. This manifold hence constitutes the actual input space, or the “world”, of our problem. While the manifold is not easily defined, it is tangible: for example, its dimension can be estimated based on the neighbourhoods of inputs in the data set [12–15], and was found to be around  $D \approx 14$  for MNIST, and  $D \approx 35$  for CIFAR10, compared to  $N = 784$  and  $N = 3072$ , respectively. We will call inputs *structured* if they are concentrated on a lower-dimensional manifold and thus have a lower-dimensional latent representation, which consists of the coordinates of the input within that manifold.

A complementary view on the data manifold is provided by today’s most powerful generative models, called Generative Adversarial Networks (GAN) [16]. A GAN  $\mathcal{G}$  is a neural network that is trained to take random noise as its input and to transform it into outputs that resemble a given target distribution. For example, GANs can generate realistic synthetic images of human faces [17, 18]. From this point of view, the mapping from the hidden manifold to the input space is given by the function that the GAN  $\mathcal{G}$  computes.

## A. Main results

In this paper, specifically Sec. II, we introduce a generative model for structured data sets in the above sense

\* sebastian.goldt@phys.ens.fr

† marc.mezard@ens.fr

‡ florent.krzakala@ens.fr

§ lenka.zdeborova@cea.fr

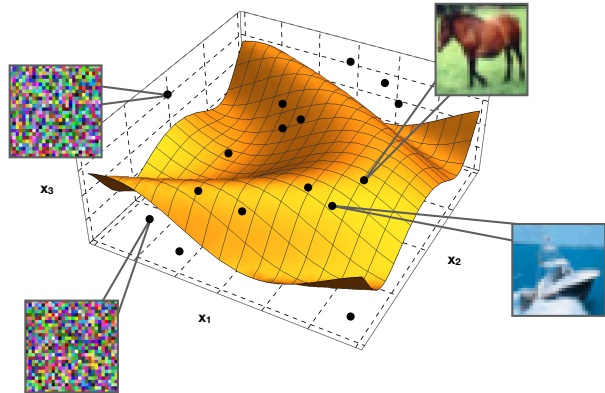


FIG. 1. We illustrate the notion of a **hidden manifold in input space** using CIFAR10 example images. Each black point indicates a possible input in a high-dimensional input space  $\mathbb{R}^N$ . Most points in this space cannot be interpreted as images at all; however, those points that can be interpreted as real images tend to concentrate on a lower-dimensional manifold, here sketched as a two-dimensional curved surface in a three-dimensional space. The intrinsic dimension  $D$  of these lower-dimensional manifolds has been measured numerically [12–15].

that we call the *hidden manifold model* (HMM). It is a generative model that produces tuples  $(\mathbf{x}, y^*)$  of high-dimensional inputs  $\mathbf{x} \in \mathbb{R}^N$  and their scalar labels  $y^*$ . The key idea is to construct the inputs such that they lie on a lower-dimensional manifold; their labels are then a function of only their position within that manifold. The way the inputs are generated is akin to a learnt single layer decoder with random inputs; it can also be viewed as a single layer generator neural network of a learnt GAN. As a result, inputs drawn from the HMM have non-trivial correlations, and the labels  $y^*$  cannot be written as a simple function of the inputs  $\mathbf{x}$ .

Our key theoretical result, presented in Sec. III, is to show that despite these correlations, the HMM is amenable to an analytical treatment in a thermodynamic limit of large dimensions  $N$  and  $D$ , large number of samples  $P$ , and fixed respective ratios  $D/N$ ,  $P/N$ . We derive the solution showing a “Gaussian Equivalence Property” (GEP). As a first application, we use the GEP to derive a set of integro-differential equations that captures the behaviour of two-layer neural networks, with  $K = \mathcal{O}(1)$  hidden units, trained using stochastic gradient descent. These equations extend the classical analysis of the dynamics of two-layer neural networks on unstructured data [19–21] to the hidden manifold and provide detailed insight into the dynamics of learning.

We then use these equations to study the dynamics and the performance of two-layer neural networks trained on data generated by the HMM, in Sec. IV. We find back the specialisation of hidden units, known from the canonical

teacher-student model. We analyse the learning for different feature matrices, and show that Hadamard matrices perform slightly better than i.i.d. Gaussian ones. We show analytically that the generalisation performance deteriorates as the manifold dimension  $D$  grows. We show that the learning rate has a very minor influence on the asymptotic error, and analyse how the error final error of the network changes as a function of the width of the hidden layer.

Sec. V is devoted to comparison of learning on the HMM and on real data sets such as MNIST [10], fashion-MNIST [22] or CIFAR10 [11]. In particular, we demonstrate that neural networks learn functions of increasing complexity over the course of training on both the HMM and real data sets. We also compare the memorisation of some samples during the early stages of training between the HMM to real data. These comparisons provide strong evidence that the HMM captures the properties of learning with one-pass SGD and two-layer neural networks on some of the standard benchmark data sets rather faithfully.

## B. Related work

*The need for models of structured data.* Several works have recognised the importance of the structure in the data sets used for machine learning, and in particular the need to go beyond the simple component-wise i.i.d. modelling [23–27]. While we will focus on the ability of neural networks to generalise from examples, two recent papers studied a network’s ability to *store* inputs with lower-dimensional structure and random labels: Chung *et al.* [28] studied the linear separability of general, finite-dimensional manifolds and their interesting consequences for the training of deep neural networks [29, 30], while Rotondo *et al.* [31] extended Cover’s classic argument [32] to count the number of learnable dichotomies when inputs are grouped in tuples of  $k$  inputs with the same label. Recently, Yoshida and Okada [33] analysed the dynamics of online learning for data having an arbitrary covariance matrix, finding an infinite hierarchy of ODEs.

*Relation to random feature learning.* The hidden manifold model has an interesting link to random feature learning with unstructured i.i.d. input data. The idea of learning with random features goes back to the mechanical perceptron of the 1960s [34] and was extended into the random kitchen sinks of Rahimi and Recht [35, 36]. Remarkably, random feature learning in the same scaling limit as used in the theoretical part of this paper was analysed in several recent and concurrent works, notably in [37, 38] for ridge regression, and in [39] for max-margin linear classifiers. These papers consider full batch learning, i.e. all samples are used at the same time, which makes one difference from our online (one-pass stochastic gradient descent) analysis. Another important difference is that we study learning in a neural network with two

layers of learned weights, while the existing works study simpler linear (perceptron-type) architectures where only one layer is learned. Perhaps more importantly, in our analysis the features do not need to be random, but can be chosen deterministically or even be learnt from data using a GAN or an autoencoder. The principles underlying the analytic solution of this paper as well as [37–39] rely on the Gaussian Equivalence Property, which is stated and used independently in those papers.

*Gaussian equivalence and random matrix theory.* Special cases of the Gaussian Equivalence Property were in fact derived previously using random matrix theory in [40–43], and this equivalent Gaussian covariates mapping was explicitly stated and used in [38, 39]. This formulation has recently been extended to a broader setting of concentrated vectors encompassing data coming from a GAN in [44, 45], a version closer to our formulation.

### C. Reproducibility

We provide the full code to reproduce our experiments as well as an integrator for the equations of motion of two-layer networks online [46].

### D. Learning setup

This paper focuses on the dynamics and performance of fully-connected two-layer neural networks with  $K$  hidden units and first- and second-layer weights  $\mathbf{W} \in \mathbb{R}^{K \times N}$  and  $\mathbf{v} \in \mathbb{R}^K$ , resp. Given an input  $\mathbf{x} \in \mathbb{R}^N$ , the output of a network with parameters  $\boldsymbol{\theta} = (\mathbf{W}, \mathbf{v})$  is given by

$$\phi(\mathbf{x}; \boldsymbol{\theta}) = \sum_k^K v_k g(\mathbf{w}_k \mathbf{x} / \sqrt{N}), \quad (1)$$

where  $\mathbf{w}_k$  is the  $k$ th row of  $\mathbf{W}$ , and  $g : \mathbb{R} \rightarrow \mathbb{R}$  is the non-linear activation function of the network, acting component-wise. We study sigmoidal and ReLU networks with  $g(x) = \text{erf}(x/\sqrt{2})$  and  $g(x) = \max(0, x)$ , resp.

We will train the neural network on data sets with  $P$  input-output pairs  $(\mathbf{x}_\mu, y_\mu^*)$ ,  $\mu = 1, \dots, P$ , where we use the starred  $y_\mu^*$  to denote the *true* label of an input  $\mathbf{x}_\mu$ . Networks are trained by minimising the quadratic training error  $E(\boldsymbol{\theta}) = 1/2 \sum_{\mu=1}^P \Delta_\mu^2$  with  $\Delta_\mu = [\phi(\mathbf{x}_\mu, \boldsymbol{\theta}) - y_\mu^*]$  using stochastic (one-pass, online) gradient descent (SGD) with constant learning rate  $\eta$  and mini-batch size 1,

$$\boldsymbol{\theta}_{\mu+1} = \boldsymbol{\theta}_\mu - \eta \nabla_{\boldsymbol{\theta}} E(\boldsymbol{\theta})|_{\boldsymbol{\theta}_\mu, \mathbf{x}_\mu, y_\mu^*}. \quad (2)$$

Initial weights for both layers were always taken component-wise i.i.d. from the normal distribution with mean 0 and standard deviation  $10^{-3}$ .

The key quantity of interest is the *test error* or *generalisation error* of a network, for which we compare its

predictions to the labels given in a test set that is composed of  $P^*$  input-output pairs  $(\mathbf{x}_\mu, y_\mu^*)$ ,  $\mu = 1, \dots, P^*$  that are *not* used during training,

$$\epsilon_g(\boldsymbol{\theta}) \equiv \frac{1}{2P^*} \sum_{\mu}^{P^*} [\phi(\mathbf{x}_\mu, \boldsymbol{\theta}) - y_\mu^*]^2. \quad (3)$$

The test set in our setting is generated by the same probabilistic model that generated the training data.

#### 1. The canonical teacher-student model

The joint probability distribution of input-output pairs  $(\mathbf{x}_\mu, y_\mu^*)$  is inaccessible for realistic data sets such as CIFAR10, preventing analytical control over the test error and other quantities of interest. To make theoretical progress, it is therefore promising to study the generalisation ability of neural networks for data arising from a probabilistic generative model.

A classic model for data sets is the *canonical teacher-student setup* where inputs  $\mathbf{x}_\mu$  are drawn element-wise i.i.d. from the standard normal distribution and labels are given by a random, but fixed, neural network with weights  $\boldsymbol{\theta}^*$  acting on the inputs:  $y_\mu^* = \phi(\mathbf{x}_\mu, \boldsymbol{\theta}^*)$ . The network that generates the labels is called the teacher, while the network that is trained is called the student. The model was introduced by Gardner & Derrida [6], and its study has provided many valuable insights into the generalisation ability of neural networks from an average-case perspective, particularly within the framework of statistical mechanics [7–9, 47–52], and also in recent statistical learning theory works, e.g. [38, 53–55]. However, it has the notable shortcoming that its analysis crucially relies on the fact that inputs are i.i.d. Gaussians and hence uncorrelated.

## II. THE HIDDEN MANIFOLD MODEL

We now introduce a new generative probabilistic model for structured data sets with correlations. To generate a data set containing  $P$  inputs in  $N$  dimensions, we first choose  $D$  feature vectors  $\mathbf{f}_r$ ,  $r = 1, \dots, D$ . These are vectors in  $N$  dimensions and we collect them in a feature matrix  $\mathbf{F} \in \mathbb{R}^{D \times N}$ . Next we draw  $P$  vectors  $\mathbf{c}_\mu$  with random i.i.d. components drawn from the normal distribution with mean zero and unit variance and collect them in the matrix  $\mathbf{C} \in \mathbb{R}^{P \times D}$ . The vector  $\mathbf{c}_\mu$  gives the coordinates of the  $\mu$ th input on the lower-dimensional manifold spanned by the feature vectors in  $\mathbf{F}$ . We will call  $\mathbf{c}_\mu$  the *latent representation* of the input  $\mathbf{x}_\mu$ , which is given by the  $\mu$ th row of

$$\mathbf{X} = f(\mathbf{C}\mathbf{F}/\sqrt{D}) \in \mathbb{R}^{P \times N}, \quad (4)$$

where  $f$  is a non-linear function acting component-wise. In this model, the “world” of the data on which the true

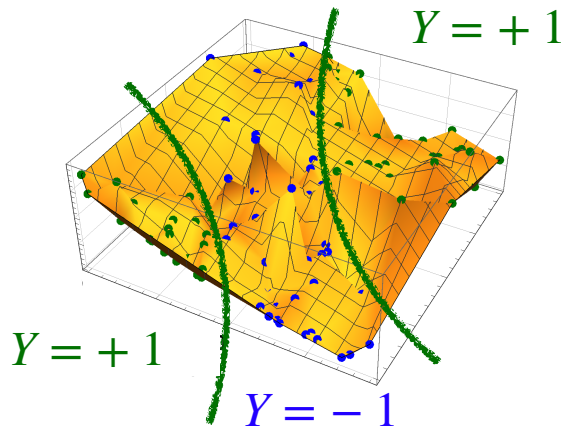


FIG. 2. **The hidden manifold model** proposed here is a generative model for structured data sets, where inputs  $\mathbf{x}$ , Eq. (4) (blue and green balls), concentrate on a lower-dimensional manifold in input space (yellow surface). Their labels  $y^*$  is a function of their position on the manifold; here we show the setup of a classification task with two classes  $y^* = \pm 1$ . In our analysis the labels are generated according to Eq. (5).

label can depend is a  $D$ -dimensional manifold, which is obtained from the linear span of  $\mathbf{F}$  through a “folding” process induced by the nonlinear function  $f$ . We note that the structure of data of the same type arises in a learned variational autoencoder network [56] with single layer, or in a learned GAN network [16] with a single layer generator network, the matrix  $C$  then corresponds to the random input, the  $F$  to the learned features,  $f$  is the corresponding output activation. The matrix  $\mathbf{F}$  can be generic with a certain normalisation, such that its elements are  $\mathcal{O}(1)$ . For our analysis to be valid, we will later assume the normalisation given in Eq. (13) and balance condition given by (12), other than that our analysis hold for arbitrary matrices  $\mathbf{F}$ .

The labels are obtained by applying a two-layer neural network with weights  $\tilde{\boldsymbol{\theta}} = (\tilde{\mathbf{W}} \in \mathbb{R}^{M \times D}, \tilde{\mathbf{v}} \in \mathbb{R}^M)$  within the unfolded hidden manifold according to

$$y_\mu^* = \phi(\mathbf{c}_\mu, \tilde{\boldsymbol{\theta}}) = \sum_m^M \tilde{v}^m \tilde{g}(\tilde{\mathbf{w}}^m \mathbf{c}_\mu / \sqrt{D}). \quad (5)$$

We draw the weights in both layers component-wise i.i.d. from the normal distribution with unity variance, unless we note it otherwise. The key point here is the dependency of labels  $y_\mu^*$  on the coordinates of the lower-dimensional manifold  $\mathbf{c}_\mu$  rather than on the high-dimensional data  $\mathbf{x}_\mu$ . We expect the exact functional form of this dependence not to be crucial for the empirical part of this work, and that there are other forms that would present the same behaviour. Notably it would be interesting to consider ones where the latent representation is conditioned to the labels as in conditional

GANs [57] or the manifold model of [30].

### III. THE SOLUTION OF THE HIDDEN MANIFOLD MODEL

#### A. The Gaussian Equivalence Property

The difficulty in analysing HMM comes from the fact that the various components of one given input pattern, say  $x_{\mu i}$  and  $x_{\nu j}$ , are correlated. Yet, a key feature of the model is that it is amenable to an analytical treatment. To that end, we will be studying the standard thermodynamic limit of the statistical physics of learning where the size of the input space  $N \rightarrow \infty$ , together with the number  $P \rightarrow \infty$  of patterns that are presented for learning, while keeping the ratio  $\alpha \equiv P/N$  fixed. In statistics this corresponds to the challenging high-dimensional limit. The hidden manifold model can then be studied analytically if one assumes that the latent dimension  $D$ , i.e. the dimension of the feature space, also scales with  $N$ , meaning that it goes to  $\infty$  with a fixed ratio  $\delta \equiv D/N$  which is of order 1 with respect to  $N$ , so that we have

$$N, P, D \rightarrow \infty, \quad \text{with fixed } \alpha \equiv \frac{P}{N} \text{ and } \delta \equiv \frac{D}{N}. \quad (6)$$

In this limit, the relevant variables are the “local fields” or pre-activations that are acted upon by the neurons in the hidden layer. They can be shown to follow a Gaussian distribution in the thermodynamic limit (6). We will now make this statement precise by formulating a “Gaussian Equivalence Property” (GEP). We will demonstrate the power of this equivalence by deriving a set of exact equations for online learning in Sec. III B.

*Statement of the Property* Let  $\{C_r\}_{r=1}^D$  be  $D$  i.i.d. Gaussian random variables distributed as  $\mathcal{N}(0, 1)$ . In the following we shall denote by  $\mathbb{E}$  the expectation value with respect to this distribution. Define  $N$  variables  $u_i$ ,  $i = 1, \dots, N$  as linear superpositions of the  $C_r$  variables,

$$u_i \equiv \frac{1}{\sqrt{D}} \sum_{r=1}^D C_r F_{ir}, \quad (7)$$

and  $M$  variables  $\nu^m$ ,  $m = 1, \dots, M$  as other linear superpositions,

$$\nu^m \equiv \frac{1}{\sqrt{D}} \sum_{r=1}^D C_r \tilde{w}_r^m, \quad (8)$$

where  $\tilde{w}_r^m$  are the teacher weights Eq. (5). Define  $K$  variables  $\lambda^k$  as linear superpositions of  $f(u_i)$  where  $f$  is an arbitrary function:

$$\lambda^k \equiv \frac{1}{\sqrt{N}} \sum_{i=1}^N w_i^k f(u_i), \quad (9)$$

where  $\tilde{w}_i^k$  are the student weights Eq. (1). Denoting by  $\langle g(u) \rangle$  the expectation of a function  $g(u)$  when  $u$  is a

normal variable with distribution  $u \sim \mathcal{N}(0, 1)$ , we also introduce for convenience the ‘‘centered’’ variables

$$\tilde{\lambda}^k \equiv \frac{1}{\sqrt{N}} \sum_{i=1}^N w_i^k (f(u_i) - \langle f(u) \rangle). \quad (10)$$

Notice that our notations keeps upper indices for indices which take values in a finite range ( $k, \ell \in \{1, \dots, K\}$ ,  $m, n \in \{1, \dots, M\}$ ), and lower indices for those which have a range of order  $N$  ( $i, j \in \{1, \dots, N\}$ ;  $r, s \in \{1, \dots, D\}$ ).

As the  $C_r$  are Gaussian, the  $u_i$  variables are also Gaussian variables, with mean zero and a matrix of covariance

$$U_{ij} = \mathbb{E}[u_i u_j] = \frac{1}{D} \sum_{r=1}^D F_{ir} F_{jr}. \quad (11)$$

We assume that, in the thermodynamic limit, the  $\mathbf{W}$ ,  $\tilde{\mathbf{W}}$  and  $\mathbf{F}$  matrices have elements of  $\mathcal{O}(1)$  and that they are ‘‘balanced’’ in the sense that  $\forall p, q \geq 1$ ,  $\forall k_1, \dots, k_p, r_1, \dots, r_q$ , we have

$$\begin{aligned} S_{r_1 r_2 \dots r_q}^{k_1 k_2 \dots k_p} \\ = \frac{1}{\sqrt{N}} \sum_i w_i^{k_1} w_i^{k_2} \dots w_i^{k_p} F_{ir_1} F_{ir_2} \dots F_{ir_q} = \mathcal{O}(1), \end{aligned} \quad (12)$$

with the  $q$  and  $p$  distinct. We also have a similar scaling for the combinations involving the teacher weights  $\tilde{w}_r^m$ . We also assume that for  $i \neq j$ ,

$$\frac{1}{\sqrt{D}} \sum_{r=1}^D F_{ir} F_{jr} = \mathcal{O}(1), \quad \text{and} \quad \sum_{r=1}^D (F_{ir})^2 = D. \quad (13)$$

Notice that the only variables which are drawn i.i.d. from a Gaussian distribution are the coefficients  $C_r$ . Most importantly, the matrices  $\mathbf{F}$  and  $\mathbf{W}$  can be arbitrary (and deterministic) as long as they are balanced.

Note that the covariances of the  $u_i$  variables scale in the thermodynamic limit as

$$\mathbb{E}[u_i^2] = 1; \quad \mathbb{E}[u_i u_j] = \mathcal{O}(1/\sqrt{D}), \quad i \neq j. \quad (14)$$

Under these conditions:

**Property III.1. Gaussian Equivalence Property (GEP)** *In the asymptotic limit when  $N \rightarrow \infty$ ,  $D \rightarrow \infty$ , keeping  $K, M$  and the ratio  $D/N$  finite,  $\{\lambda^k\}$  and  $\{\nu^m\}$  are  $K + M$  jointly Gaussian variables, with mean*

$$\mathbb{E}[\lambda^k] = a \frac{1}{\sqrt{N}} \sum_{i=1}^N w_i^k; \quad \mathbb{E}[u^m] = 0, \quad (15)$$

and covariance

$$Q^{k\ell} \equiv \mathbb{E}[\tilde{\lambda}^k \tilde{\lambda}^\ell] = (c - a^2 - b^2) W^{k\ell} + b^2 \Sigma^{k\ell}, \quad (16)$$

$$R^{km} \equiv \mathbb{E}[\tilde{\lambda}^k \nu^m] = b \frac{1}{D} \sum_{r=1}^D S_r^k \tilde{w}_r^m, \quad (17)$$

$$T^{mn} \equiv \mathbb{E}[\nu^m \nu^n] = \frac{1}{D} \sum_{r=1}^D \tilde{w}_r^m \tilde{w}_r^n, \quad (18)$$

The ‘‘folding function’’  $f(\cdot)$  appears through the three coefficients  $a, b, c$ , which are defined as

$$a \equiv \langle f(u) \rangle, \quad b \equiv \langle u f(u) \rangle, \quad c \equiv \langle f(u)^2 \rangle \quad (19)$$

where  $\langle \psi(u) \rangle$  denotes the expectation value of the function  $\psi$  when  $u \sim \mathcal{N}(0, 1)$  is a Gaussian variable.

The covariances are defined in terms of the three matrices

$$S_r^k \equiv \frac{1}{\sqrt{N}} \sum_{i=1}^N w_i^k F_{ir}, \quad (20)$$

$$W^{k\ell} \equiv \frac{1}{N} \sum_{i=1}^N w_i^k w_i^\ell, \quad (21)$$

$$\Sigma^{k\ell} \equiv \frac{1}{D} \sum_{r=1}^D S_r^k S_r^\ell, \quad (22)$$

whose elements are assumed to be of order  $\mathcal{O}(1)$  in the asymptotic limit.

The derivation of the property is given in Appendix A. This Gaussian equivalence property shows that there is a whole family of activation functions  $f(x)$  (those that have the same values for  $a, b$  and  $c$  from Eq. 19) that will lead to equivalent analytical results for the learning curves studied in this paper. Furthermore, it forms a basis from which we can develop an analytical understanding of learning with the hidden manifold model, as we show in the next section.

Before moving to an application of the GEP, let us briefly review some related results. A special case of the Gaussian Equivalence Property was in fact known in random matrix theory [37, 40–44] and the mapping was explicitly used in [38, 39]. We stress that the GEP does not require the matrix  $\mathbf{F}$  to be a random one, and is valid as well for deterministic matrices, as long as the balanced conditions stated in Eqs. (12-13) hold. This allows to generalise these mappings to the case of deterministic features using Hadamard and Fourier matrices, such as the one used in Fastfood [58] or ACDC [59] layers. These orthogonal projections are actually known to be more effective than the purely random ones [60]. It also allows generalisation of the analysis in this paper for data coming from a learned GAN, along the lines of [44, 45]. We shall illustrate this point below by analysing the dynamics of online learning when the feature matrix  $\mathbf{F}$  is a deterministic Hadamard matrix (cf. Sec. IV B).

## B. The dynamics of stochastic gradient descent for the Hidden Manifold Model

To illustrate the power of the GEP, we now analyse the dynamics of stochastic gradient descent (2) in the case of *online learning*, where at each step of the algorithm  $\mu = 1, 2, \dots$ , the student’s weights are updated according to Eq. (2) using a previously unseen sample  $(\mathbf{x}_\mu, y_\mu)$ .

This case is also known as one-shot or single-pass SGD. The analysis of online learning has been performed previously for the canonical teacher-student model with i.i.d. Gaussian inputs [19–21, 61, 62], and has recently been put on a rigorous foundation [51]. Here, we generalise this type of analysis to two-layer neural networks trained on the Hidden Manifold Model. To keep our notation light, we focus on even functions  $f(u)$ , such that  $a = 0$  (19). Extending our results to  $a \neq 0$  is straightforward.

The goal of our analysis is to track the mean-squared generalisation error of the student with respect to the teacher at all times,

$$\epsilon_g(\boldsymbol{\theta}, \tilde{\boldsymbol{\theta}}) \equiv \frac{1}{2} \mathbb{E} [\phi(\mathbf{x}, \boldsymbol{\theta}) - \tilde{y}^*]^2, \quad (23)$$

where the expectation  $\mathbb{E}$  denotes an average over an input drawn from the hidden manifold model, Eq. (4), with label  $y_\mu^* = \phi(\mathbf{c}_\mu, \tilde{\boldsymbol{\theta}}^*)$  given by a teacher network with fixed weights  $\tilde{\boldsymbol{\theta}}^*$  acting on the latent representation, Eq. (5). Note that the weights of both the student and the teacher, as well as the feature matrix  $F_{ir}$ , are held fixed when taking the average, which is an average only over the coefficients  $c_{\mu r}$ . To keep notation compact, we focus on cases where  $a = \mathbb{E} f(u) = 0$  in (19), which leads to  $\tilde{\lambda}^k = \lambda^k$  in (10). A generalisation to the case where  $a \neq 0$  is straightforward but lengthy.

We can make progress with the high-dimensional average over  $\mathbf{x}$  in Eq. (23) by noticing that the input  $\mathbf{x}$  and its latent representation  $\mathbf{c}$  only enter the expression via the local fields  $\nu^m$  and  $\lambda^k$ , Eqs. (8, 9):

$$\epsilon_g(\boldsymbol{\theta}, \tilde{\boldsymbol{\theta}}) = \frac{1}{2} \mathbb{E} \left( \sum_k^K v^k g(\lambda^k) - \sum_m^M \tilde{v}^m \tilde{g}(\nu^m) \right)^2 \quad (24)$$

The average is now taken over the joint distribution of local fields  $\{\lambda^{k=1,\dots,K}, \nu^{m=1,\dots,M}\}$ . The key step is then to invoke the Gaussian Equivalence Property III.1, which guarantees that this distribution is a multivariate normal distribution with covariances  $Q^{k\ell}$ ,  $R^{km}$ , and  $T^{nm}$  (16–18). Depending on the choice of  $g(x)$  and  $\tilde{g}(x)$ , this makes it possible to compute the average analytically; in any case, the GEP guarantees that we can express  $\epsilon_g(\boldsymbol{\theta}, \tilde{\boldsymbol{\theta}})$  as a function of only the second-layer weights  $v^k$  and  $\tilde{v}^m$  and the matrices  $Q^{k\ell}$ ,  $R^{km}$ , and  $T^{nm}$ , which are called *order parameters* in statistical physics [19–21]:

$$\lim_{N,D \rightarrow \infty} \epsilon_g(\boldsymbol{\theta}, \tilde{\boldsymbol{\theta}}) = \epsilon_g(Q^{k\ell}, R^{kn}, T^{nm}, v^k, \tilde{v}^m) \quad (25)$$

where in taking the limit, we keep the ratio  $\delta \equiv D/N$  finite (see Eq. 6). For example, for a student with  $g(\lambda^k) = \text{erf}(\lambda^k/\sqrt{2})$  and a teacher with  $\tilde{g}(\nu^m) = \max(0, \nu^m)$ , we find that

$$\begin{aligned} \epsilon_g(Q^{k\ell}, R^{kn}, T^{nm}, v^k, \tilde{v}^m) &= \frac{1}{\pi} \sum_{i,k} v_i v_k \arcsin \left( \frac{Q^{ik}}{\sqrt{1+Q^{ii}} \sqrt{1+Q^{kk}}} \right) - \sum_{k,n} v_k \tilde{v}^n \frac{R^{kn}}{\sqrt{2\pi} \sqrt{1+Q^{kk}}} \\ &+ \sum_{n,m} \tilde{v}^n \tilde{v}^m \frac{2\sqrt{T^{mm}T^{nn} - (T^{nm})^2} + T^{nm} \left[ \pi + 2 \arctan \left( \frac{T^{nm}}{\sqrt{T^{mm}T^{nn} - (T^{nm})^2}} \right) \right]}{8\pi}. \end{aligned} \quad (26)$$

### 1. The physical interpretation of the order parameters

The order parameter  $R^{kn}$ , defined in (17, 20), measures the similarity between the action of the  $i$ th student node on an input  $\mathbf{x}_\mu$  and the  $n$ th teacher node acting on the corresponding latent representation  $\mathbf{c}_\mu$ . In the canonical teacher-student setup, where (i) the input covariance is simply  $\mathbb{E} x_i x_j = \delta_{ij}$  and (ii) labels are generated by the teacher acting directly on the inputs  $\mathbf{x}$ , it can be readily verified that the overlap has the simple expression  $R^{kn} \equiv \mathbb{E} \lambda^k \nu^n \sim \mathbf{w}^k \tilde{\mathbf{w}}^n$ . It was hence called the teacher-student overlap in the previous literature. In the HMM, however, where teacher and student network act on different vector spaces, it is not *a priori* clear how to express the teacher-student overlap in suitable order parameters.

The matrix  $Q^{k\ell} = [c - b^2] W^{k\ell} + b^2 \Sigma^{k\ell}$  quantifies the similarity between two student nodes  $k$  and  $\ell$ , and has two contributions: the latent student-student overlap  $\Sigma^{k\ell}$ , which measures the overlap of the weights of two students nodes after they have been projected to the hidden manifold, and the ambient student-student overlap  $W^{k\ell}$ , which measures the overlap between the vectors  $\mathbf{w}^k, \mathbf{w}^\ell \in \mathbb{R}^N$ . Finally, we also have the overlaps of the teacher nodes are collected in the matrix  $T^{nm}$ , which is *not* time-dependent, as it is a function of the teacher weights only.

## 2. Statement of the equations of motion

We have derived a closed set of equations of motion that describe the dynamics of the order parameters  $R^{km}$ ,  $\Sigma^{k\ell}$ ,  $W^{k\ell}$  and  $v^k$  when the student is trained using online SGD (2). We stress at this point that in the online learning, at each step of SGD a new sample is given to the network. The weights of the network are thus uncorrelated to this sample, and hence the GEP can be applied at every step. This is in contrast with the full-batch learning where the correlations between weights and inputs have to be taken into account explicitly [39]. Integrating the equations of motion and substituting the values of the order parameters into Eq. (25) gives the generalisation error at all times. Here, we give a self-contained statement of the equations, and relegate the details of the derivation to Appendix B;

A key object in our analysis is the spectrum of the matrix

$$\Omega_{rs} \equiv \frac{1}{N} \sum_i F_{ir} F_{is}. \quad (27)$$

We denote its eigenvalues and corresponding eigenvectors by  $\rho$  and  $\psi_\rho$ , and write  $p_\Omega(\rho)$  for the distribution of eigenvalues. It turns out that it is convenient to rewrite the teacher-student overlap as an integral over a density  $r^{km}(\rho, t)$ , which is a function of  $\rho$  and of the normalised number of steps  $t = P/N$ , which can be interpreted as a continuous time-like variable. We then have

$$R^{km}(t) = b \int d\rho p_\Omega(\rho) r^{km}(\rho, t). \quad (28)$$

with  $b \equiv \langle uf(u) \rangle$  (19). In the canonical teacher-student model, introducing such a density and the integral that comes with it is not necessary, but in the HMM is a consequence of the non-trivial correlation matrix  $\mathbb{E} x_i x_j$  between input elements. Adopting the convention that the indices  $j, k, \ell, \iota = 1, \dots, K$  always denote *student* nodes, while  $n, m = 1, \dots, M$  are reserved for teacher hidden nodes. The equation of motion of the teacher-student density can then be written as

$$\begin{aligned} \frac{\partial r^{km}(\rho, t)}{\partial t} = & -\frac{\eta}{\delta} v^k d(\rho) \left( r^{km}(\rho) \sum_{j \neq k}^K v^j \frac{Q^{jj} I_3(k, k, j) - Q^{kj} I_3(k, j, j)}{Q^{jj} Q^{kk} - (Q^{kj})^2} + \sum_{j \neq k}^K v^j r^{jm}(\rho) \frac{Q^{kk} I_3(k, j, j) - Q^{kj} I_3(k, k, j)}{Q^{jj} Q^{kk} - (Q^{kj})^2} \right. \\ & + v^k r^{km}(\rho) \frac{1}{Q^{kk}} I_3(k, k, k) - r^{km}(\rho) \sum_n^M \tilde{v}^n \frac{T^{nn} I_3(k, k, n) - R^{kn} I_3(k, n, n)}{Q^{kk} T^{nn} - (R^{kn})^2} \\ & \left. - \frac{b\rho}{d(\rho)} \sum_n^M \tilde{v}^n \tilde{T}^{nm} \frac{Q^{kk} I_3(k, n, n) - R^{kn} I_3(k, k, n)}{Q^{kk} T^{nn} - (R^{kn})^2} \right), \end{aligned} \quad (29)$$

where  $d(\rho) = (c - b^2)\delta + b^2\rho$ . The teacher-teacher overlap  $T^{nm} \equiv \mathbb{E} \nu^n \nu^m$  (18), while  $\tilde{T}^{nm}$  is the overlap of the teacher weights after rotation into the eigenbasis of  $\Omega_{rs}$ , weighted by the eigenvalues  $\rho$ :

$$\tilde{T}^{mn} \equiv \frac{1}{D} \sum_\tau \rho_\tau \tilde{\omega}_\tau^m \tilde{\omega}_\tau^n; \quad \text{where} \quad \tilde{\omega}_\tau^m = \frac{1}{\sqrt{D}} \sum_r \tilde{w}_r^m \psi_{\tau r}. \quad (30)$$

In writing the equations, we used the following shorthand for the three-dimensional Gaussian averages

$$I_3(k, j, n) \equiv \mathbb{E} [g'(\lambda^k) \lambda^j \tilde{g}(\nu^n)], \quad (31)$$

which was introduced by Saad & Solla [21]. Arguments passed to  $I_3$  should be translated into local fields on the right-hand side by using the convention where the indices  $j, k, \ell, \iota$  always refer to student local fields  $\lambda^j$ , etc., while the indices  $n, m$  always refer to teacher local fields  $\nu^n, \nu^m$ . Similarly,

$$I_3(k, j, j) \equiv \mathbb{E} [g'(\lambda^k) \lambda^j g(\lambda^j)], \quad (32)$$

where having the index  $j$  as the third argument means that the third factor is  $g(\lambda^j)$ , rather than  $\tilde{g}(\nu^m)$  in Eq. (31). The average in Eq. (31) is taken over a three-dimensional normal distribution with mean zero and covariance matrix

$$\Phi^{(3)}(k, j, n) = \begin{pmatrix} Q^{kk} & Q^{kj} & R^{kn} \\ Q^{kj} & Q^{jj} & R^{jn} \\ R^{kn} & R^{jn} & T^{nn} \end{pmatrix}. \quad (33)$$

For the latent student-student overlap  $\Sigma^{k\ell}$ , it is again convenient to introduce the density  $\sigma^{k\ell}(\rho, t)$  as

$$\Sigma^{k\ell}(t) = \int d\rho p_{\Omega}(\rho) \sigma^{k\ell}(\rho, t), \quad (34)$$

whose equation of motion is given by

$$\begin{aligned} \frac{\partial \sigma^{k\ell}(\rho, t)}{\partial t} = & -\frac{\eta}{\delta} \left( d(\rho) v^k \sigma^{k\ell}(\rho) \sum_{j \neq k} v^j \frac{Q^{jj} I_3(k, k, j) - Q^{kj} I_3(k, j, j)}{Q^{jj} Q^{kk} - (Q^{kj})^2} + v^k \sum_{j \neq k} v^j d(\rho) \sigma^{j\ell}(\rho) \frac{Q^{kk} I_3(k, j, j) - Q^{kj} I_3(k, k, j)}{Q^{jj} Q^{kk} - (Q^{kj})^2} \right. \\ & + d(\rho) v^k \sigma^{k\ell}(\rho) v^k \frac{1}{Q^{kk}} I_3(k, k, k) - d(\rho) v^k \sigma^{k\ell}(\rho) \sum_n \tilde{v}^n \frac{T^{nn} I_3(k, k, n) - R^{kn} I_3(k, n, n)}{Q^{kk} T^{nn} - (R^{kn})^2} \\ & - b \rho v^k \sum_n \tilde{v}^n r^{\ell n}(\rho) \frac{Q^{kk} I_3(k, n, n) - R^{kn} I_3(k, k, n)}{Q^{kk} T^{nn} - (R^{kn})^2} \\ & \left. + \text{all of the above with } \ell \rightarrow k, k \rightarrow \ell \right) \\ & + \eta^2 v^k v^{\ell} \left[ (c - b^2) \rho + \frac{b^2}{\delta} \rho^2 \right] \left( \sum_{j, \iota}^K v^j v^{\iota} I_4(k, \ell, j, \iota) \right. \\ & \left. - 2 \sum_j^K \sum_m^M v^j \tilde{v}^m I_4(k, \ell, j, m) + \sum_{n, m}^M \tilde{v}^n \tilde{v}^m I_4(k, \ell, n, m) \right). \end{aligned} \quad (35)$$

This equation involves again the integrals  $I_3$  and a four-dimensional average that we denote

$$I_4(k, \ell, j, n) \equiv \mathbb{E} [g'(\lambda^k) g'(\lambda^{\ell}) g(\lambda^j) g(\nu^n)]. \quad (36)$$

using the same notational conventions as for  $I_3$ , so the four-dimensional covariance matrix reads

$$\Phi^{(4)}(k, \ell, j, n) = \begin{pmatrix} Q^{kk} & Q^{k\ell} & Q^{kj} & R^{kn} \\ Q^{k\ell} & Q^{\ell\ell} & Q^{\ell j} & R^{\ell n} \\ Q^{kj} & Q^{\ell j} & Q^{jj} & R^{jn} \\ R^{kn} & R^{\ell n} & R^{jn} & T^{nn} \end{pmatrix}. \quad (37)$$

The equation of motion for the ambient student-student overlap  $W^{k\ell}$  can be written directly:

$$\begin{aligned} \frac{dW^{k\ell}(t)}{dt} = & -\eta v^k \left( \sum_j^K v^j I_3(k, \ell, j) - \sum_n \tilde{v}^n I_3(k, \ell, n) \right) - \eta v^{\ell} \left( \sum_j^K v^j I_3(\ell, k, j) - \sum_n \tilde{v}^n I_3(\ell, k, n) \right) \\ & + c \eta^2 v^k v^{\ell} \left( \sum_{j, a}^K v^j v^a I_4(k, \ell, j, a) - 2 \sum_j^K \sum_m^M v^j \tilde{v}^m I_4(k, \ell, j, m) + \sum_{n, m}^M \tilde{v}^n \tilde{v}^m I_4(k, \ell, n, m) \right). \end{aligned} \quad (38)$$

Finally, the ODE for the second-layer weights  $v^k$  is straightforwardly given by

$$\frac{dv^k}{dt} = \eta \left[ \sum_n^M \tilde{v}^n I_2(k, n) - \sum_j^K v^j I_2(k, j) \right], \quad (39)$$

where we have introduced the final short-hand  $I_2(k, j) \equiv \mathbb{E} [g(\lambda^k) g(\lambda^j)]$ .

### 3. Solving the equations of motion

The equations of motion are valid for any choice of  $f(x)$ ,  $g(x)$  and  $\tilde{g}(x)$ . To solve the equations for a particular setup, one needs to compute the three constants  $a, b, c$  (19) and the averages  $I_3$  and  $I_4$  (31, 36). Choosing  $g(x) =$



$\tilde{g}(x) = \text{erf}(x/\sqrt{2})$ , they can be computed analytically [20]. Finally, one needs to determine the spectral density of the matrix  $\Omega_{rs}$ . When drawing the entries of the feature matrix  $F_{ir}$  i.i.d. from some probability distribution with finite second moment, the limiting distribution of the eigenvalues  $p_\Omega(\rho)$  in the integral (28) and (34) is the Marchenko-Pastur distribution [63]:

$$p_{\text{MP}}(\rho) = \frac{1}{2\pi\delta} \frac{\sqrt{(\rho_{\text{max}} - \rho)(\rho - \rho_{\text{min}})}}{\rho}, \quad (40)$$

where  $\rho_{\text{min}} = (1 - \sqrt{\delta})^2$  and  $\rho_{\text{max}} = (1 + \sqrt{\delta})^2$ , where we recall that  $\delta \equiv D/N$ . Note that our theory crucially also applies to non-random matrices; we will visit such an example in Sec. IV B, where we also discuss the importance of this use case.

At this point, we remind the reader that a complete numerical implementation of the equations of motion is available on GitHub [46].

#### IV. ANALYTICAL RESULTS

The goal of this section is to use the analytic description of online learning to analyse the dynamics and the performance of two-layer neural networks in detail.

##### A. Specialisation of student nodes in the HMM

We start by illustrating the content of the equations of motion in Fig. 3, where we plot the dynamics of the generalisation error, the order parameters  $R^{km}$ ,  $\Sigma^{k\ell}$  and  $W^{k\ell}$  and the second-layer weights  $v^k$  obtained from a single experiment with  $N = 10000$ ,  $D = 100$ ,  $M = K = 2$ , starting from small initial weights (crosses). The elements of the feature matrix are drawn i.i.d. from the standard normal distribution, as are the elements of the latent representations  $\mathbf{c}$ . The solid lines give the dynamics of these order parameters obtained by integrating the equations of motion. The initial conditions for the integration of the ODEs were taken from the simulation.

The first thing to notice is that the ODE description matches this single experiment really well even at moderate system sizes. For Fig. 3, our choice of  $N$  and  $D$  results in  $\delta = 0.01$ , and we checked that the ODEs and simulations agree for various values of  $\delta$ , *cf.* Fig. 5.

An intriguing feature of both the canonical teacher-student setup and the hidden manifold model is that they both exhibit a *specialisation* phenomenon. Upon closer inspection of the time evolution of the order parameter  $R^{km}$  in Fig. 3 (b), we see that during the initial decay of the generalisation error up to a time  $t = P/N \sim 10$ , all elements of the matrix  $R^{km}$  are comparable. In other words, the correlations between the pre-activation  $\lambda^k$  of any student node and the pre-activation  $\nu^m$  of any teacher node is roughly the same. As training continues, the student nodes “specialise”: the pre-activation of one student node becomes strongly correlated with the pre-activation of only a single teacher node. In the example shown in Fig. 3, we have strong correlations between the pre-activation of the first student and the first teacher node ( $R^{11}$ ), and similarly between the second student

and second teacher node ( $R^{22}$ ). The specialisation of the teacher-student correlations is concurrent to a decorrelation of the student units, as can be seen from the decay of the off-diagonal elements of the latent and ambient student-student overlaps  $\Sigma^{k\ell}$  and  $W^{k\ell}$ , respectively (bottom of Fig. 3). Similar specialisation transitions have been observed in the canonical teacher-student setup for both online and batch learning [21, 64]; see Engel and Van den Broeck [8] for a review.

##### B. Using non-random feature matrices

Our first example of the learning dynamics in Sec. IV A was for a feature matrix  $\mathbf{F}$  whose entries were taken i.i.d. from the normal distribution. However, the derivation of the ODEs for online learning does not require that the feature matrix  $\mathbf{F}$  be random; instead, it only requires the balance condition stated in Eq. (12) as well as the normalisation conditions (13). To illustrate this point, we plot examples of online learning dynamics with  $M = K = 2$  in Fig. 4, with the prediction from the ODE as solid lines and the result of a single simulation with crosses. In blue, we show results where the elements of  $F_{ir}$  were drawn i.i.d. from the standard normal distribution. For the experiment in orange,  $\mathbf{F} = \mathbf{H}_N$ , where  $\mathbf{H}_N$  is a Hadamard matrix [65]. Hadamard matrices are  $N \times N$  matrices, hence  $\delta = 1$ , and are popular in error-correcting codes such as the Reed-Muller code [66, 67]. They can be defined via the relation

$$\mathbf{H}_N \mathbf{H}_N^\top = N \mathbb{I}_N, \quad (41)$$

where  $\mathbb{I}_N$  is the  $N \times N$  identity matrix. As we can see from Fig. 4, the ODEs capture the generalisation dynamics of the Hadamard-case just as well.

##### C. The limit of small latent dimension

The key technical challenge in analysing the analytical description of the dynamics is handling the integro-differential nature of the equations. However, we can

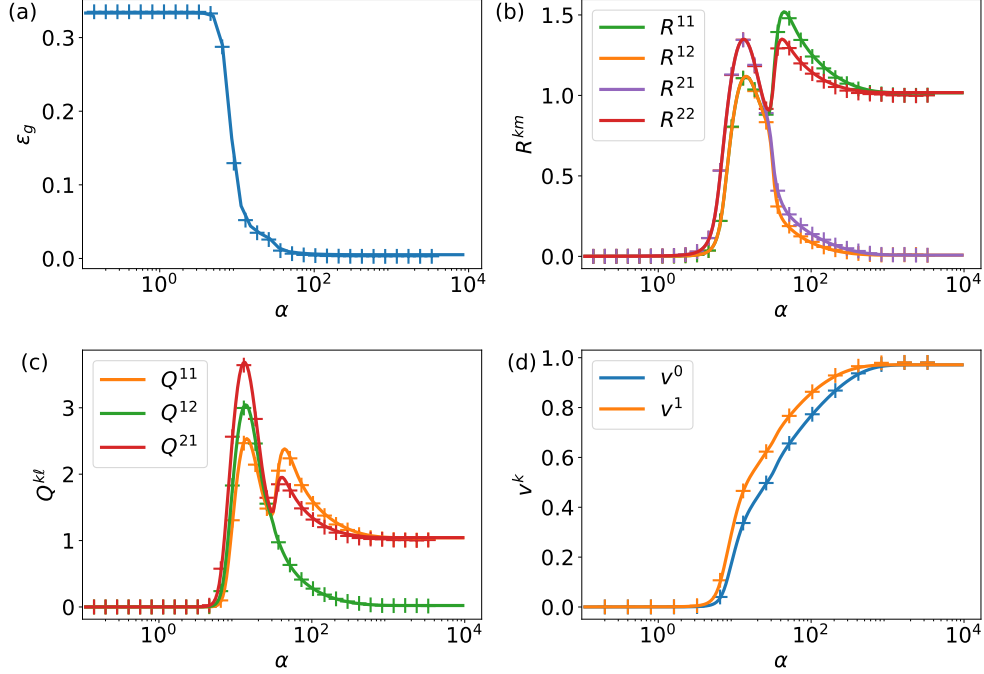


FIG. 3. **The analytical description of the hidden manifold generalisation dynamics matches experiments even at moderate system size.** We plot the time evolution of the generalisation error  $\epsilon_g(\alpha)$  and the order-parameters  $R^{km}$ ,  $Q^{kl}$  and 2nd layer weights  $v^k$  obtained by integration of the ODEs (solid) and from a single run of SGD (crosses). Parameters:  $g(x) = \text{erf}(x/\sqrt{2})$ ,  $N = 10000$ ,  $D = 100$ ,  $M = 2$ ,  $K = 2$ ,  $\eta = 0.2$ ,  $\tilde{v}^m = 1$ .

simplify the equations in the limit of small  $\delta \equiv D/N$ . Numerical integration of the equations reveals that at convergence, the continuous order parameter densities  $r^{km}(\rho)$  and  $\sigma^{kl}(\rho)$  are approximately constant:

$$r^{km}(\rho) = r^{km}; \quad \sigma^{kl}(\rho) = \sigma^{kl} \quad (42)$$

This is a key observation, because making the ansatz (42) allows us to transform the integro-differential equations for the dynamics of  $r^{km}(\rho, t)$  (29) and  $\sigma^{kl}(\rho, t)$  (35) into first-order ODEs, provided we can perform the integral over the eigenvalue distribution  $p_\Omega(\rho)$  in Eqs. (28) and (34) analytically. This is for example the case if we take the elements of the feature matrix  $\mathbf{F}$  i.i.d. from any probability distribution with bounded second moment, in which case  $p_\Omega(\rho)$  is given by the Marchenko-Pastur distribution (40). We will focus on this case for the remainder of this section.

Let us note that the regime of small delta is also the relevant regime for image data sets such as MNIST and CIFAR10, whose  $\delta$  has been estimated previously to be around  $\delta_{\text{MNIST}} \sim 14/784$  and  $\delta_{\text{CIFAR10}} \sim 35/3072$ , respectively [12–15]; cf. our discussion in the Introduction.

### 1. The effect of the latent dimension $D = \delta N$

As a first application of this approach, we analyse the dependence of the asymptotic test error  $\epsilon_g^*$  on the latent dimension  $D$  of the hidden manifold when teacher and student have the same number of hidden nodes,  $K = M$ .

From inspection of the form of the order parameters after integrating the full set of ODEs until convergence, we made the following ansatz for the overlap matrices:

$$\Sigma^{k\ell} = \begin{cases} S & k = \ell, \\ s & \text{otherwise,} \end{cases} \quad W^{k\ell} = \begin{cases} W & k = \ell, \\ w & \text{otherwise,} \end{cases} \quad (43)$$

$$T^{nm} = \begin{cases} T & n = m, \\ t & \text{otherwise,} \end{cases} \quad \tilde{T}^{nm} = \begin{cases} \tilde{T} & n = m, \\ \tilde{t} & \text{otherwise,} \end{cases} \quad (44)$$

$$R^{km} = \begin{cases} R & k = m, \\ r & \text{otherwise} \end{cases} \quad v^k = v; \quad A^m = A \quad (45)$$

Substituting this ansatz into the ODEs allowed us to derive a closed set of ODEs for the seven order parameters  $R, r, S, s, W, w$  and  $v$  that is valid for small  $\delta$  and for any  $K = M$ . The teacher-related order parameters  $T, t, \tilde{T}$

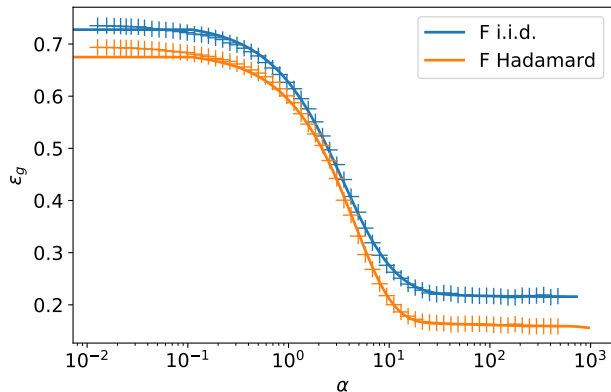


FIG. 4. **The ODE analysis is asymptotically correct for non-random feature matrices  $F$ .** We plot the time evolution of the generalisation error  $\epsilon_g$  obtained by integration of the ODEs (solid) and from a single run of SGD (2) (crosses) for two different matrices  $F$ : (i) elements  $F_{ir}$  are drawn i.i.d. from the standard normal distribution (blue); (ii)  $F$  is a Hadamard matrix [65]  $f(x) = \text{sgn}(x), g(x) = \tilde{g}(x) = \text{erf}(x/\sqrt{2}), N = 1023, D = 1023, M = 2, K = 2, \eta = 0.2, \tilde{v}^m = 1$ .

and  $\tilde{t}$  describe the teacher and are constants of the motion. They have to be chosen to reflect the distribution from which the weights of the teacher network are drawn in an experiment. The full equations of motion are rather long, so instead of printing them here in full we provide a Mathematica notebook for reference [46].

The key idea of our analytical approach is to look for fixed points of this ODE system and to substitute the values of the order parameters at those fixed points into the expression for the generalisation error (25). To understand the structure of the fixed points of the ODEs, we ran a numerical fixed point search of the ODEs from 1000 initial values for the order parameters drawn randomly from the uniform distribution. We found two types of fixed points. First, there exists an un-specialised fixed point with  $R = r, S = s$  and  $W = w$ . This corresponds to the initial phase of learning discussed in Sec. IV A, when networks with  $K > 1$  hidden nodes have not yet specialised and hence achieve only the performance of a network with  $K = 1$  hidden unit. The second fixed point shows specialisation, *i.e.* we have  $R$  large and  $r$  small, etc. This is the fixed point that is reached asymptotically at the end of online learning, and substituting the values of the order parameters at that fixed point into Eq. (25) yields the asymptotic generalisation error of a student.

We show the results of this analysis in Fig. 5. The crosses are experimental results for which we trained networks with  $M = K = 2$  on data from a hidden manifold with latent dimension  $D = 25, 50, 100$  and  $200$ , choosing the input dimension  $N$  to obtain the range of  $\delta$  desired for each curve. We plot the asymptotic error averaged over

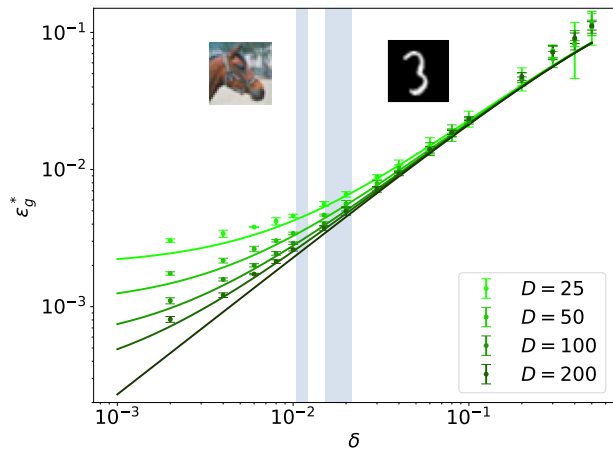


FIG. 5. **The impact of the latent dimension  $\delta \equiv D/N$ .** We plot the final test error  $\epsilon_g^*$  of sigmoidal students trained on the hidden manifold model with three different intrinsic dimensions  $D$  as a function of  $\delta = D/N$ , where  $N$  is the input dimension. The average is taken over five runs. The solid lines are the asymptotic theoretical predictions derived in Sec. IV C 1. The shaded bars indicate experimental estimates [12–15] for  $\delta$  for the CIFAR10 data set (left) and the MNIST data set (right).  $f(x) = \text{sgn}(x), g(x) = \tilde{g}(x) = \text{erf}(x/\sqrt{2}), M = K = 2, \eta = 0.2, \tilde{v}^m = 1$

five runs with dots; error bars indicated two standard deviations. The lowest solid line in Fig. 5 is the theoretical prediction obtained by the procedure just explained when assuming that  $T = 1, t = 0, \tilde{T} = 1, \tilde{t} = 0$ .

While the experimental results are approaching the theoretical line as the latent dimension  $D$  increases, there are qualitative differences in the shape of the  $\delta$  dependence for small  $\delta$ . These differences arise due to the following finite-size effect. While it is numerically easy to enforce  $T = 1, t = 0$  by orthogonalising the teacher weight matrix, it is not possible to explicitly control the re-weighted teacher-teacher overlap  $\tilde{T}^{nm}$  (30). The deviation of  $\tilde{T}^{nm}$  from the identity lead to the deviations we see at small  $\delta$ . We demonstrate this in Fig. 5 by also plotting theoretical predictions for  $\tilde{T} = 1 - x, \tilde{t} = x$  and choosing  $x = 1/D$ . These curves match the experiments much better. Plotting the data with a linear y-scale (not shown) reveals that the solution obtained making the small- $\delta$  ansatz (42) is valid until  $\delta \sim 0.2$ .

## 2. Learning rate $\eta$

In the inset of Fig. 6, we plot the generalisation dynamics of a neural network trained on the HMM at different learning rates. Two observations stand out. As expected, the learning rate controls the speed of learning, with increased learning rates leading to faster learning until the learning rate becomes so large that learning is not possible anymore; instead, the weights just grow to infinity.

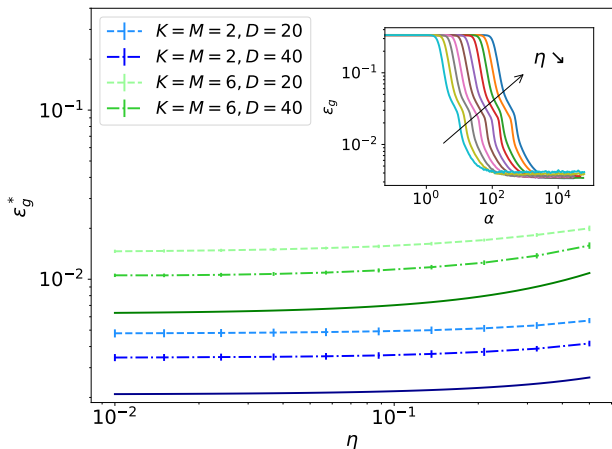


FIG. 6. **The impact of the learning rate  $\eta$ .** We plot the final test error  $\epsilon_g^*$  of sigmoidal students trained on the hidden manifold model for a range of learning rates  $\eta$  for sigmoidal networks with  $K = M = 2$  (blue) and  $K = M = 6$  (green). We repeated the experiments for two values of  $D$ , choosing  $N$  such that  $\delta = D/N = 0.01$ . (Inset) Generalisation dynamics during training ( $K = M = 2$ ). Parameters:  $f(x) = \text{sgn}(x)$ ,  $g(x) = \tilde{g}(x) = \text{erf}(x/\sqrt{2})$ ,  $\delta = 0.01$ ,  $\tilde{v}^m = 1$ ,  $K = M$ .

The asymptotic test error  $\epsilon_g^*$ , however, does depend only very weakly on the learning rate. We focus on this asymptotic error in the main part of the plot, where we show it as a function of  $\eta$  for  $M = K = 2$  and  $M = K = 6$ , together with the theoretical prediction for  $\tilde{t} = 0$ . This theoretical prediction is again obtained by using the ansatz (43) for the order parameters and solving the resulting fixed point equations, as described in the previous section, but this time varying the learning rate  $\eta$ .

The weak dependence of  $\epsilon_g$  on  $\eta$  should be contrasted with the behaviour the canonical teacher-student setup, where the generalisation error is proportional to the learning rate in the case of additive Gaussian output noise [51, 68].

### 3. The impact of student size

Another key question in our model is how the performance of the student depends on her number of nodes  $K$ . Adding hidden units to a student who has less hidden units than her teacher ( $K < M$ ) improves her performance, as would be expected. This can be understood in terms of the specialisation discussed in Sec. IV A: each additional hidden node of the student specialises to another node of the teacher, leading to improved performance. We will see an example of this below in Sec. V A.

But what happens if we give the student more nodes than her teacher has  $K > M$ ? It is instructive to first study the overlap matrices at the end of training. We show two examples from an experiment with

$M = 2, K = 6$  at  $\delta = 0.01$  for networks starting from different initial conditions. In particular, we plot the rescaled teacher-student overlap matrix  $v^k R^{km}$  in Fig. 7 (b, c). We rescale  $R^{km}$  by the second-layer weights to account for two effects: first, the relative influence of a given node to the output of the student, which is determined by the magnitude of the corresponding second-layer weight; and second, we have a symmetry in the output of the student since for sigmoidal activation function,  $v^k g(\mathbf{w}^k \mathbf{x} / \sqrt{N}) = -v^k g(-\mathbf{w}^k \mathbf{x} / \sqrt{N})$ .

It is clear from the two plots that for  $K > M$ , the student nodes display *many-to-one* specialisation: several hidden units of the student specialise to the same hidden node of the teacher, essentially providing several estimates of the value of this teacher node. We found this pattern of activations consistently across all of our runs, and they motivate the following ansatz for the ODEs:

$$R^{km} = \begin{cases} R & k \bmod M = m \bmod M, \\ r & \text{otherwise} \end{cases} \quad (46)$$

$$\Sigma^{k\ell} = \begin{cases} S & k \bmod M = \ell \bmod M, \\ s & \text{otherwise} \end{cases} \quad (47)$$

and similarly for  $W^{k\ell}$ , while we use the same parameterisation for the teacher order parameters  $T, t, \tilde{T}, \tilde{t}, A$  and  $v$ . Searching again for specialised fixed points of the resulting equations for the seven time-dependent order parameters  $R, r, S, s, W, w$  and  $v$  and substituting their values into Eq. (25) yields the predictions we indicate by solid lines in Fig. 7, where we plot the asymptotic test error as a function of  $Z \equiv K/M$ . We can see small performance improvements as the student size increases. We also plot, for the three values of  $M$  used, the asymptotic test error measured in experiments with  $D = 50, 100$  and 200. As we increase  $D$ , the experimental results approach the theoretical prediction for  $D \rightarrow \infty$ .

We finally note that fixed points of the online dynamics with many-to-one specialisation have been described previously in the canonical teacher-student setup by Goldt *et al.* [51], who found that this behaviour leads to a more significant improvement of student performance as  $K$  increases for teacher tasks with  $y^* = \phi(\mathbf{x})$  compared to the improvement we observe for the HMM. The same type of many-to-one specialisation was also found by Mei *et al.* [69] and Chizat and Bach [70], who considered a complementary regime where the input dimension  $N$  stays finite while the size of the hidden layer goes to infinity.

## V. COMPARING THE HIDDEN MANIFOLD MODEL TO REAL DATA

We finally turn our attention to the comparison of the hidden manifold model to more realistic data sets, in our cases classic image databases such as CIFAR10 (see Fig. 1 for two examples of images in CIFAR10).

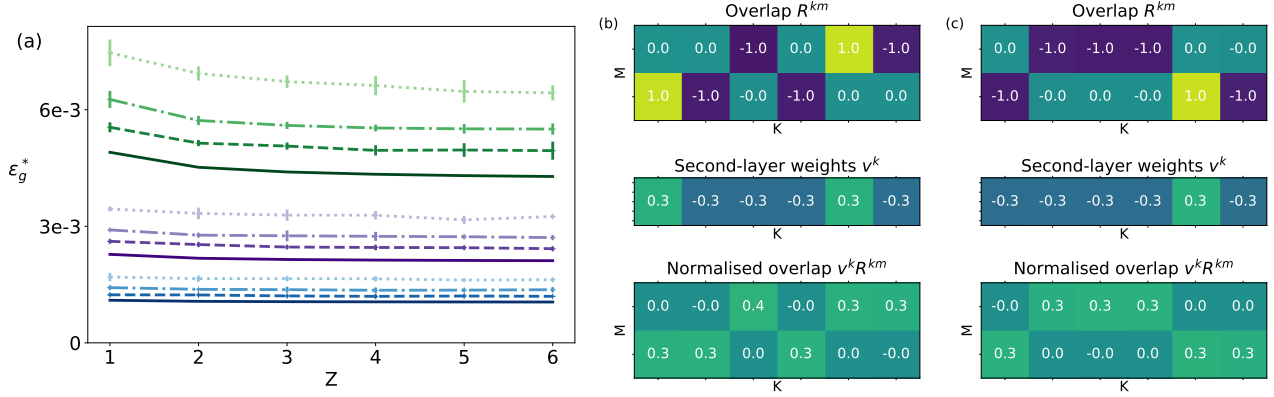


FIG. 7. (a) **Asymptotic generalisation for online learning** of a student with  $K = ZM$  hidden nodes learning from a teacher with  $M = 1$  (blue),  $M = 2$  (violet) and  $M = 4$  (green) hidden nodes, respectively. The dotted, dashed-dotted and dashed lines correspond to  $D = 50, 100$  and  $200$ , respectively. Error bars indicated two standard deviations over five runs. The solid line is the theoretical prediction obtained for  $\tilde{t} = 0$ . (b, c) Teacher-student overlap  $R^{km}$  (17), second-layer weights  $v^k$  and the normalised overlap  $v^k R^{km}$  obtained in two simulations used in the left plot with  $M = 2, K = 6$ , starting from different initial conditions, all other things being equal. *Parameters:* In all plots,  $f(x) = \text{sgn}(x), g(x) = \text{erf}(x/\sqrt{2}), \eta = 0.2, \tilde{v}^m = 1, \delta = 0.01, \eta = 0.2$ .

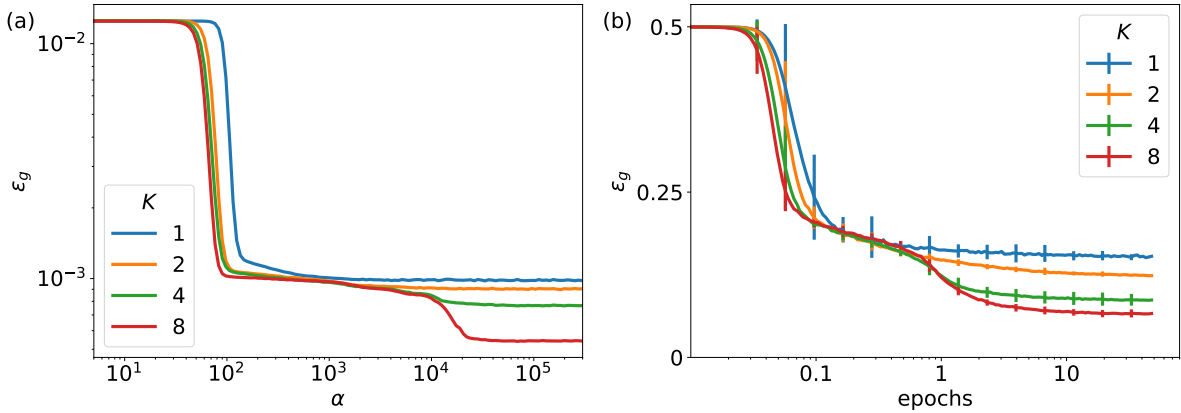


FIG. 8. **Two-layer neural networks learn functions of increasing complexity.** We plot the generalisation error of sigmoidal two-layer networks with increasing number of hidden nodes  $K$  during a single run of online learning from a teacher with  $M = 10, \tilde{v}^m = 1/M$  on the HMM (a) and when trained on odd-versus-even digit classification on MNIST, averaged over ten runs (b). Error bars indicate two standard deviations. For details, see Sec. V A and D.  $g(x) = \text{erf}(x/\sqrt{2}), \eta = 0.2, N = 784$ . (b): batch size 32.

### A. Neural networks learn functions of increasing complexity

The specialisation transition that we discussed in Sec. IV A has an important consequence for the performance of the neural network, as we show in Fig. 8. As we train increasingly large student networks on a teacher with  $M = 10$  hidden units and second-layer weights  $\tilde{v}^m = 1/M$ , we observe that learning proceeds in two phases. First, there is an initial decay of the generalisation error until all students have roughly the same test error as the student with a single hidden unit  $K = 1$ . In a second phase, students with  $K > 1$  break away from

this plateau after further training and achieve superior performance, with the larger networks performing better. These improvements are a result of specialisation after  $\sim 10^3$  epochs, which permits the student network to capitalise on their additional hidden nodes.

This way of visualising specialisation not only illustrates its importance for student performance, it is also applicable when training the same two-layer neural networks on more realistic data sets such as MNIST (Fig. 8 b) or Fashion MNIST [22] and CIFAR (Fig. 10). The plots demonstrate clearly that in all these cases, the larger networks proceed by first learning functions that are equivalent to the smaller networks.

In all cases, specialisation is preceded by a plateau where the generalisation error stays constant because the student is stuck at a saddle point in its optimisation landscape, corresponding to the unspecialised solution. This plateau has been discussed extensively in the canonical teacher-student setup [8, 61, 71, 72] and more recently in the context of recurrent and deep neural networks [73, 74]. By comparing students of different sizes, this plateau can also be demonstrated on image data sets, as we have done above. This learning of functions with increasing complexity has also been observed in deep convolutional networks by Kalimeris *et al.* [75], who used quantities from information theory to quantify how well one model explains the performance of another.

These observations are interesting because they suggest how to explain the ability of neural networks to generalise well from examples when they have *many more* parameters than samples in their training data set. This is a key open problem in the theory of deep learning, since the intuition from classical statistics suggests that in these cases, the networks overfit the training data and thus generalise poorly [5, 76]. It is possible that by learning functions of increasing complexity, networks are biased towards simple classifiers and avoid over-fitting if their training is stopped before convergence. This topic is an active research area [77, 78].

## B. Memorisation of random and realistic data

An interesting difference between random and realistic data was demonstrated in a recent paper by Arpit *et al.* [79]. They trained 100 two-layer ReLU networks ( $K = 4096$  hidden units, 10 output units with softmax activation function) for a single epoch on the ten-class image classification task on the CIFAR10 data set, starting from different initial conditions each time. At the end of training, they measured the frequency with which each individual image was classified correctly by the network across runs, which we will call the memorability of an image, which should be thought of as a function of the image and the data set that contains it. We repeated this experiment on the following four data sets (colour codes refer to Fig. 9):

**CIFAR10:**  $\mathbf{x}_\mu$ : CIFAR10 images,  $y_\mu^*$ : CIFAR10 labels

**Gaussian:** teacher acting on Gaussian inputs:  $\mathbf{x}_\mu$  i.i.d. standard Gaussians,  $y_\mu^* = \phi(\mathbf{x}_\mu, \boldsymbol{\theta}^*)$

**TeacherS:** teacher acting on structured inputs  $\mathbf{x}_\mu = f(\mathbf{F}\mathbf{c}_\mu)$ ,  $y_\mu^* = \phi(\mathbf{x}_\mu, \boldsymbol{\theta}^*)$

**HMM:**  $\mathbf{x}_\mu = f(\mathbf{F}\mathbf{c}_\mu)$ ,  $y_\mu^* = \phi(\mathbf{c}_\mu, \boldsymbol{\theta}^*)$

The labels for the synthetic data sets were generated by two teacher networks, one with input dimension  $N$  for the Gaussian and TeacherS data sets, and another with input dimension  $D$  for the HMM. Both teachers were

fully connected networks with  $M = 2K$  hidden units and ReLU activation function.

We plot the memorabilities for all images in the training set, sorted by their memorability, in Fig. 9. On the left, we first reproduce the memorability curve for CIFAR10 that was found by Arpit *et al.* [79] (solid blue), which demonstrates that many examples are *consistently* classified correctly or incorrectly after a single epoch of training. The memorability curve for a data set containing the same images with *random* labels (dashed blue) demonstrates that randomised CIFAR10 doesn't contain images that are particularly hard or easy to memorise. The smaller variation in memorability for the randomised data set is largely due to the fact that it takes it more time to fit randomised data sets [80]. After one epoch, the network thus has a lower training accuracy on the randomised data set (cf. the inset of Fig. 9), which leads to the smaller area underneath the curve. We verified that no easy or hard samples appear when training the randomised data sets to comparable training accuracy (not shown). In fact, the memorability of data sets with random labels seem to coincide after accounting for differences in the training error, regardless of whether the inputs are CIFAR10 images, Gaussian inputs or structured inputs  $\mathbf{X} = f(\mathbf{CF})$  (4) (dashed lines in Fig. 9 a).

The memorability curves for the Gaussian, TeacherS and HMM data sets in Fig. 9 (b) reveal that hard and easy examples exist for TeacherS and HMM, which both contain structured inputs  $\mathbf{X} = f(\mathbf{CF})$ , but not in the Gaussian data set. The number of easy examples, but not their existence, correlates well with the training accuracy on these data sets, shown in the inset. In that sense, the hidden manifold model is thus a more realistic model of image-like data than the canonical teacher-student setup.

Note that by making the teacher network larger than the students ( $M = 2K$ ), the learning problem is unrealisable for all three synthetic data sets, *i.e.* there is no set of weights for the student that achieve zero generalisation error. The absence of easy examples in the Gaussian data set thus suggests that unrealisability alone is insufficient to obtain a data set with easy examples. Our results also demonstrate that memorability is not just a function of the input correlations: CIFAR10 images, Gaussian inputs and structured inputs yield the same memorability curves when their labels are randomised. We leave it to future work to identify some criterion, statistical or otherwise, that predicts either whether a sample  $(\mathbf{x}_\mu, y_\mu^*)$  is easy (or hard!) to memorise or whether a training set contains easy examples at all.

## VI. CONCLUDING PERSPECTIVES

We have introduced the hidden manifold model as a generative model for structured data sets that displays some of the phenomena that we observe when training two-layer neural networks on realistic data. The HMM has two key ingredients, namely high-dimensional inputs

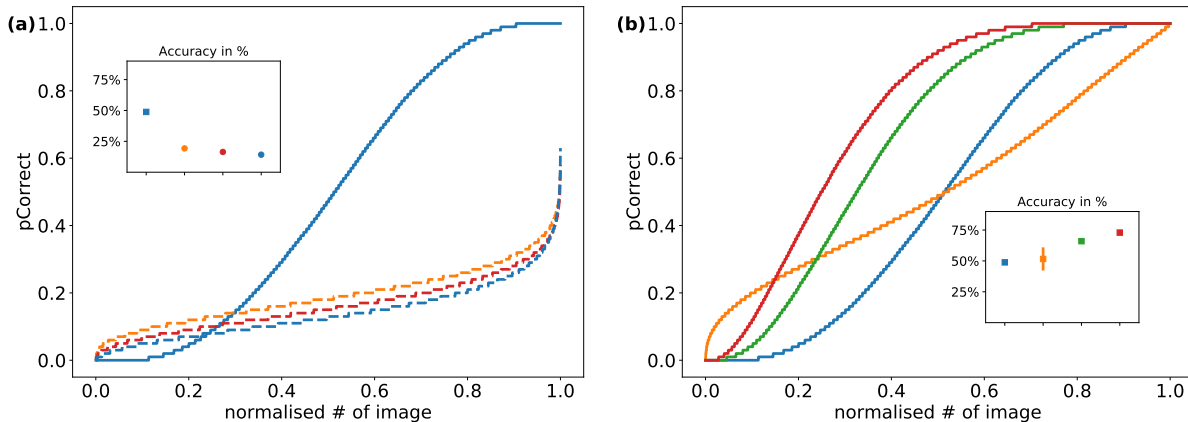


FIG. 9. **Neural networks have different memorisation patterns for random and structured data sets.** We plot the memorability of training images, i.e. the frequency with which an image from the training set is correctly classified by a neural network after training for only a single epoch. In Figs. (a) and (b), the full blue line is the CIFAR10 result from Arpit *et al.* [79], which shows the existence of hard and easy examples which are never, or always, classified correctly. Fig. (b) shows that these hard and easy examples also exist in the structured data models, *TeacherS* and the *HMM*, but not in the unstructured *Gaussian* one. Fig. (a) shows that this property disappears in all models when the labels are reshuffled (dashed lines). The insets indicate the training accuracy after training, using circles for randomised data sets and squares for unmodified data sets.

which lie on a lower-dimensional manifold, and labels for these inputs that depend on the inputs' position within the low dimensional manifold. We derived an analytical solution of the model for online SGD learning of two-layer neural networks. We thus provide a rich test bed for exploring the influence of data structure on learning in neural networks.

Let us close this paper by outlining several important directions in which our work is being (or should be) extended.

*Comparison to more deep learning phenomenology* In the spirit of our experiments in Section V, it is of great interest to identify more properties of learning that are consistently reproduced across experiments with realistic data sets and network architectures, and to test whether the HMM reproduces these observations as well. Of particular interest will be those cases where learning on realistic data deviates from the HMM, and how we can extend the HMM to capture these behaviours.

*Beyond online SGD* Our analytical results on online SGD rely on the assumption that each new sample seen during training is conditionally independent from the weights of the network up to that point. In practice, samples are seen several or even many times during training, giving rise to additional correlations. Taking those correlations into account to analyse those cases is an important future direction. First steps towards a solution to this challenging problem were made using the dynamical replica method [81, 82] for two-layer networks, and for single-layer neural networks trained using full-batch gradient descent, where all the samples in the training set are used at every step of the algorithm [38, 39, 83]. Generalising these results to two-layer networks is clearly a direction for future work as well.

*Learning with a multi-layer network* The present work should be extended to learning with multi-layer networks in order to identify how depth helps to deal with structured data. This is a serious challenge, and it remains an open problem to find explicitly solvable models of multi-layer (non-linear) networks even in the canonical canonical teacher-student model where inputs are uncorrelated.

*Multi-layer generative model* The hidden manifold model is akin to a single layer generator of a GAN. A natural extension would be to take a generator with an arbitrary number of layers. Multi-layer generators are explored in [37, 45], whose results are analogous to the Gaussian equivalence property and suggest that the full solution of the online SGD or of the full-batch gradient descent might also be within reach.

*Conditioning the inputs on the labels* In the HMM, the true label  $y^*$  of an input  $x$  is conditioned on its latent representation  $c$ , i.e. its coordinates in the manifold. It may be more realistic to consider models where instead, the latent representation is conditioned on the label of the input, i.e.  $p(c|y)$ . A simple case of such a model that reduces to a Gaussian mixture of two clusters was explored recently [84]. This is also the point of view taken implicitly in [30]. More generally, exploring different approaches to modelling realistic inputs will allow us to better understand how data structure influences learning.

## ACKNOWLEDGMENTS

We would like to thank Bruno Loureiro and Federica Gerace for useful discussions. We thank Stanislaw Jas-

trzębski for discussing the experiments of [79]. We are grateful to the Kavli Institute For Theoretical Physics for its hospitality during an extended stay, during which parts of this work were conceived and carried out. We acknowledge funding from the ERC under the European Union’s Horizon 2020 Research and Innovation Pro-

gramme Grant Agreement 714608-SMiLe, from “Chaire de recherche sur les modèles et sciences des données”, Fondation CFM pour la Recherche-ENS, and from the French National Research Agency (ANR) grant PAIL. This research was supported in part by the National Science Foundation under Grant No. NSF PHY-1748958

## Appendix A: The Gaussian Equivalence Property

### 1. Nonlinear functions of weakly correlated Gaussian random variables

In order to derive the GEP we first establish some auxiliary lemmas concerning the correlations between nonlinear functions of weakly correlated random variables.

#### a. Correlations of two functions

**Lemma A.1.** *Given  $n + p$  random variables organised in two vectors,*

$$x = \begin{pmatrix} x^1 \\ \vdots \\ x^n \end{pmatrix}, \quad y = \begin{pmatrix} y^1 \\ \vdots \\ y^p \end{pmatrix}, \quad (\text{A1})$$

with a joint Gaussian distribution, denote by  $\mathbb{E}$  the expectation with respect to this distribution. The first moments are supposed to vanish,

$$\mathbb{E} x_i = 0, \quad \mathbb{E} y_j = 0, \quad (\text{A2})$$

and we denote by  $Q, R, \varepsilon S$  the covariances:

$$\mathbb{E} [x_i x_j] = Q_{ij}, \quad \mathbb{E} [y_i y_j] = R_{ij}, \quad \mathbb{E} [x_i y_j] = \varepsilon S_{ij}. \quad (\text{A3})$$

Let  $f(x)$  and  $g(y)$  be two functions of  $x$  and  $y$  respectively regular enough so that  $\mathbb{E}_x[x_i f(x)]$ ,  $\mathbb{E}_x[x_i x_j f(x)]$ ,  $\mathbb{E}_y[y_i f(y)]$  and  $\mathbb{E}_y[y_i y_j f(y)]$  exist, where  $\mathbb{E}_x$  denotes the expectation with respect to the distribution  $\mathcal{N}(a, Q)$  of  $x$  and  $\mathbb{E}_y$  denotes the expectation with respect to the distribution  $\mathcal{N}(b, R)$  of  $y$ .

Then, in the  $\varepsilon \rightarrow 0$  limit:

$$\mathbb{E} [f(x)g(y)] = \mathbb{E}_x[f(x)] \mathbb{E}_y[g(y)] + \varepsilon \sum_{i=1}^n \sum_{j=1}^p \mathbb{E}_x[x_i f(x)] (Q^{-1} S R^{-1})_{ij} \mathbb{E}_y[y_j g(y)] + \mathcal{O}(\varepsilon^2). \quad (\text{A4})$$

*Proof.* The result is obtained by a straightforward expansion in  $\varepsilon$ .

The joint distribution of  $x$  and  $y$  is

$$P(x, y) = \frac{1}{Z} \exp \left[ -\frac{1}{2} \begin{pmatrix} x & y \end{pmatrix} M^{-1} \begin{pmatrix} x \\ y \end{pmatrix} \right] \quad (\text{A5})$$

where

$$M = \begin{pmatrix} Q & \varepsilon S \\ \varepsilon S^T & R \end{pmatrix}. \quad (\text{A6})$$

One can expand the inverse matrix  $M^{-1}$  to first order in  $\varepsilon$ :

$$M^{-1} = \begin{pmatrix} Q^{-1} & 0 \\ 0 & R^{-1} \end{pmatrix} - \varepsilon \begin{pmatrix} 0 & Q^{-1} S R^{-1} \\ R^{-1} S^T Q^{-1} & 0 \end{pmatrix} \quad (\text{A7})$$



and substitute this into the joint distribution (A5) to find

$$P(x, y) = \frac{1}{Z} \exp \left[ -\frac{1}{2} (x \ y) \begin{pmatrix} Q^{-1} & 0 \\ 0 & R^{-1} \end{pmatrix} \begin{pmatrix} x \\ y \end{pmatrix} \right] \left[ 1 + \varepsilon \sum_{i=1}^n \sum_{j=1}^p x_i (Q^{-1} S R^{-1})_{ij} y_j + \mathcal{O}(\varepsilon^2) \right]. \quad (\text{A8})$$

Using this expression, the result (A4) follows immediately.  $\square$

An immediate application of the lemma to the case when  $n = p = 1$  is the following. Consider two Gaussian random variables  $u_1, u_2$  with mean zero and covariance

$$\mathbb{E}[u_1^2] = 1 \quad ; \quad \mathbb{E}[u_2^2] = 1 \quad ; \quad \mathbb{E}[u_1 u_2] = \varepsilon m_{12}, \quad (\text{A9})$$

and two functions  $f_1$  and  $f_2$ . Define, for  $i \in \{1, 2\}$ :

$$a_i = \langle f_i(u) \rangle \quad ; \quad b_i = \langle u f_i(u) \rangle \quad (\text{A10})$$

where  $\langle \cdot \rangle$  denotes the average over the distribution of the random Gaussian variable  $u$  distributed as  $\mathcal{N}(0, 1)$ .

Then, in the  $\varepsilon \rightarrow 0$  limit, the correlation between  $f(u_1)$  and  $g(u_2)$  is given by

$$\mathbb{E}[f_1(u_1) f_2(u_2)] = a_1 a_2 + \varepsilon m_{12} b_1 b_2 + \mathcal{O}(\varepsilon^2). \quad (\text{A11})$$

This means that, if we consider centered functions  $\tilde{f}_i(u_i) = f_i(u_i) - a_i$ , their covariance is

$$\mathbb{E}[\tilde{f}_1(u_1) \tilde{f}_2(u_2)] = +\varepsilon m_{12} b_1 b_2 + \mathcal{O}(\varepsilon^2). \quad (\text{A12})$$

This result generalises to correlation functions of higher order, as stated in the following lemma.

#### b. Higher-order correlations

**Lemma A.2.** Consider  $m$  Gaussian random variables  $u_1, \dots, u_m$  with mean zero and covariance

$$\forall i : \mathbb{E}[u_i^2] = 1, \quad \forall i \neq j : \mathbb{E}[u_i u_j] = \varepsilon m_{ij}, \quad (\text{A13})$$

and  $m$  functions  $f_1, \dots, f_m$ . Define as before:

$$a_i = \langle f_i(u) \rangle, \quad b_i = \langle u f_i(u) \rangle, \quad i \in \{1, \dots, m\} \quad (\text{A14})$$

and define the centered functions as

$$\tilde{f}_i(u) = f_i(u) - a_i, \quad (\text{A15})$$

then

$$\lim_{\varepsilon \rightarrow 0} \frac{1}{\varepsilon^{m/2}} \mathbb{E} \tilde{f}_1(u_1) \dots \tilde{f}_m(u_m) = \begin{cases} \sum_{\sigma \in \Pi} m_{\sigma_1 \sigma_2} m_{\sigma_{p-1} \sigma_p} & \text{if } p \text{ is even} \\ = 0 & \text{if } p \text{ is odd} \end{cases} \quad (\text{A16})$$

where  $\Pi$  denotes all the  $m!/(2^{m/2}(m/2)!)$  partitions of  $\{1, \dots, m\}$  into  $m/2$  disjoint pairs. This result means that, for the moments involving only different indices, the random variables  $\tilde{f}_1(u_1)/\sqrt{\varepsilon}, \dots, \tilde{f}_m(u_m)/\sqrt{\varepsilon}$  behave, in the  $\varepsilon \rightarrow 0$  limit, like Gaussian variables with a covariance matrix  $b_i b_j m_{ij}$ .

*Proof.* The covariance matrix  $U$  of the variables  $u_1, \dots, u_m$  has elements 1 on the diagonal, and elements of order  $\varepsilon$  out of the diagonal:  $U = \mathbb{I} + \varepsilon m$ . One can expand  $U^{-1}$  in powers of  $\varepsilon$ :

$$U^{-1} = \sum_{p=0}^{\infty} (-\varepsilon)^p m^p. \quad (\text{A17})$$

The integration measure over the variables  $u_1, \dots, u_m$  can be expanded as:

$$\sqrt{(2\pi)^m \det M} e^{-\frac{1}{2} \sum_i u_i^2} \prod_{p=1}^{\infty} G_p(u_1, \dots, u_m) \quad (\text{A18})$$

where

$$G_p(u_1, \dots, u_m) = 1 + \left(-\frac{\varepsilon}{2}\right)^p \sum_{ij} (m^p)_{ij} u_i u_j + \frac{1}{2!} \left(-\frac{\varepsilon}{2}\right)^{2p} \sum_{ijkl} (m^p)_{ij} (m^p)_{kl} u_i u_j u_k u_l + \dots \quad (\text{A19})$$

When we compute the integral of  $\tilde{f}_1(u_1) \dots \tilde{f}_m(u_m)$  with the measure (A18), because of the fact that  $\langle \tilde{f}_i(u_i) \rangle = 0$ , we need to include terms coming from  $\prod_p G_p(u_1, \dots, u_p)$  that involve at least one power of each of the variables  $u_1, \dots, u_m$ .

When  $m$  is even, say  $m = 2r$ , for  $\varepsilon \rightarrow 0$ , the term of this kind with the smallest power of  $\varepsilon$  is the monomial  $u_1 \dots u_{2r}$  that comes from the  $r$ th order term in  $G_1$ . This gives:

$$\mathbb{E} f_1(u_1) \dots f_{2r}(u_{2r}) = \frac{1}{r!} \left(\frac{\varepsilon}{2}\right)^r \sum_{i_1 j_1 \dots i_r j_r} m_{i_1 j_1} m_{i_r j_r} + \mathcal{O}(\varepsilon^{r+1}), \quad (\text{A20})$$

where the sum  $\sum_{i_1 j_1 \dots i_r j_r}$  runs over all permutations of the indices  $1, \dots, 2r$ . This leads to (A16) for  $m$  even.

When  $m$  is odd,  $m = 2r + 1$ , for  $\varepsilon \rightarrow 0$ , the leading terms coming from  $\prod G_p$  that give a non-zero result are monomials of the type  $u_1^4 u_2 \dots u_{2r+1}$ . They are of order  $\mathcal{O}(\varepsilon^{r+1})$ . This proves (A16) for  $m$  odd.  $\square$

**Corollary A.3.** *In the special case  $m = 3$ , we get*

$$\mathbb{E} [f_1(u_1) f_2(u_2) f_3(u_3)] = a_1 a_2 a_3 + \varepsilon (a_1 m_{23} b_2 b_3 + a_2 m_{13} b_1 b_3 + a_3 m_{12} b_1 b_2). \quad (\text{A21})$$

## 2. Derivation of the Gaussian Equivalence Property

The derivation is based on the computation of moments of the variables  $\lambda^k$  and  $\nu^m$ , showing that, in the thermodynamic limit, all the moments are those of Gaussian random variables. Here we shall explicit the derivation up to fourth order moments, and leave the daunting higher order moments for a future formal proof of the GEP.

### a. Covariances

We first compute the covariance matrix  $G^{k\ell} = \mathbb{E}[\tilde{\lambda}^k \tilde{\lambda}^\ell]$ :

$$G^{k\ell} = \frac{1}{N} \sum_{i,j} w_i^k w_j^\ell \mathbb{E} (f(u_i) - a)(f(u_j) - a) \quad (\text{A22})$$

$$= (c - a^2) W^{k\ell} + \frac{1}{N} \sum_{i \neq j} w_i^k w_j^\ell \mathbb{E} (f(u_i) - a)(f(u_j) - a). \quad (\text{A23})$$

In the last piece, we need to compute  $\mathbb{E}[(f(u_i) - a)(f(u_j) - a)]$  for two Gaussian random variables  $u_i$  and  $u_j$  which are weakly correlated in the large  $N$  limit. In fact, as  $i \neq j$ :

$$\mathbb{E} u_i u_j = U_{ij} \quad (\text{A24})$$

is of order  $1/\sqrt{D}$ . In the thermodynamic limit, we can apply the lemma (A.1) which gives:

$$\mathbb{E} f(u_i) f(u_j) = a^2 + b^2 \frac{1}{D} \sum_{r=1}^D F_{ir} F_{jr}. \quad (\text{A25})$$

From Eqns. (A23) and (A25), we get the covariance of  $\lambda$  variables as written in (16). The covariance  $\mathbb{E}[\nu^m \nu^m]$  is analogous.

We now compute the covariance  $\mathbb{E}[\tilde{\lambda}^k \nu^m]$ . This is equal to

$$\frac{1}{\sqrt{N}} \sum_{i=1}^N w_i^k \frac{1}{\sqrt{D}} \sum_{r=1}^D \tilde{w}_r^m \mathbb{E} [f(u_i) C_r]. \quad (\text{A26})$$

The two variables  $u_i$  and  $c_r$  are Gaussian random variables with a correlation

$$\mathbb{E} [u_i C_r] = \frac{1}{\sqrt{D}} F_{ir} \quad (\text{A27})$$

which goes to zero as  $\mathcal{O}(1/\sqrt{N})$  in the thermodynamic limit. We can thus use Lemma (A.1), and more precisely Eq. (A12), to get

$$\mathbb{E}[f(u_i)C_r] = \frac{1}{\sqrt{D}}F_{ir}\langle uf(u)\rangle\langle C_r^2\rangle = \frac{b}{\sqrt{D}}F_{ir}. \quad (\text{A28})$$

Using this result in (A26) gives Eq. (17).

b. *Fourth moments of  $\tilde{\lambda}^k$  variables*

We study the fourth moment defined as:

$$G^{k_1 k_2 k_3 k_4} = \langle \tilde{\lambda}^{k_1} \tilde{\lambda}^{k_2} \tilde{\lambda}^{k_3} \tilde{\lambda}^{k_4} \rangle = \frac{1}{N^2} \sum_{i_1, i_2, i_3, i_4} w_{i_1}^{k_1} w_{i_2}^{k_2} w_{i_3}^{k_3} w_{i_4}^{k_4} \langle \tilde{f}(u_{i_1}) \tilde{f}(u_{i_2}) \tilde{f}(u_{i_3}) \tilde{f}(u_{i_4}) \rangle \quad (\text{A29})$$

where  $\tilde{f}(u) = f(u) - a$  is the centered function.

We shall decompose the sum over  $i_1, i_2, i_3, i_4$  depending on the number of distinct indices there are.

a. *Distinct indices* Let us study the first piece of the fourth moment  $\langle \lambda^{k_1} \lambda^{k_2} \lambda^{k_3} \lambda^{k_4} \rangle$ :

$$G_4^{k_1 k_2 k_3 k_4} = \frac{1}{N^2} \sum'_{i_1, i_2, i_3, i_4} w_{i_1}^{k_1} w_{i_2}^{k_2} w_{i_3}^{k_3} w_{i_4}^{k_4} \langle \tilde{f}(u_{i_1}) \tilde{f}(u_{i_2}) \tilde{f}(u_{i_3}) \tilde{f}(u_{i_4}) \rangle \quad (\text{A30})$$

where the sum runs over four indices  $i_1, i_2, i_3, i_4$  which are distinct from each other. We can use the factorisation property of the 4th moments of  $f(u)$  of lemma (A.2). This gives

$$\begin{aligned} G_4^{k_1 k_2 k_3 k_4} &= \frac{1}{N^2} \sum'_{i_1, i_2, i_3, i_4} w_{i_1}^{k_1} w_{i_2}^{k_2} w_{i_3}^{k_3} w_{i_4}^{k_4} \left[ \langle \tilde{f}(u_{i_1}) \tilde{f}(u_{i_2}) \rangle \langle \tilde{f}(u_{i_3}) \tilde{f}(u_{i_4}) \rangle + 2 \text{ perm.} \right] \\ &= \left( \left[ \frac{1}{N} \sum'_{i_1, i_2} w_{i_1}^{k_1} w_{i_2}^{k_2} \langle f(u_{i_1}) f(u_{i_2}) \rangle \right] \left[ \frac{1}{N} \sum'_{i_3, i_4} w_{i_3}^{k_3} w_{i_4}^{k_4} \langle f(u_{i_3}) f(u_{i_4}) \rangle \right] - \text{Corr.} \right) \\ &\quad + 2 \text{ perm.} . \end{aligned} \quad (\text{A31})$$

The correction terms come from pieces where the intersection between  $\{i_1, i_2\}$  and  $\{i_3, i_4\}$  is non-empty. If we first neglect this correction, we find

$$G_4^{k_1 k_2 k_3 k_4} = b^4 \left[ (\Sigma^{k_1 k_2} - W^{k_1 k_2}) (\Sigma^{k_3 k_4} - W^{k_3 k_4}) + 2 \text{ perm.} \right]. \quad (\text{A32})$$

Now we shall show that the corrections are negligible. Consider the term  $i_1 = i_3, i_2 \neq i_4$ . This gives a correction

$$- \frac{1}{N^2} \sum'_{i_1, i_2, i_4} w_{i_1}^{k_1} w_{i_2}^{k_2} w_{i_1}^{k_3} w_{i_4}^{k_4} \left[ \langle \tilde{f}(u_{i_1}) \tilde{f}(u_{i_2}) \rangle \langle \tilde{f}(u_{i_1}) \tilde{f}(u_{i_4}) \rangle \right]. \quad (\text{A33})$$

Using (A12)

$$\langle \tilde{f}(u_{i_1}) \tilde{f}(u_{i_2}) \rangle = b^2 U_{i_1 i_2} = b^2 \frac{1}{D} \sum_{r=1}^D F_{i_1 r} F_{i_2 r}, \quad (\text{A34})$$

we get the expression for the correction

$$- \frac{1}{N^2 D^2} \langle uf(u) \rangle^4 \sum'_{i_1, i_2, i_4} w_{i_1}^{k_1} w_{i_2}^{k_2} w_{i_1}^{k_3} w_{i_4}^{k_4} F_{i_1 r} F_{i_2 r} F_{i_1 s} F_{i_4 s} = - \frac{1}{\sqrt{N} D^2} \sum_{r, s} S_{rs}^{k_1 k_3} S_r^{k_2} S_s^{k_4}. \quad (\text{A35})$$

Using our hypothesis on the fact that the quantities  $S$  are of order one, this correction is clearly at most of order  $\mathcal{O}(1/\sqrt{N})$ , and therefore negligible.

The last correction that we need to consider is the term where  $i_1 = i_3 = i$ , and  $i_2 = i_4 = j$ . This gives

$$- \frac{1}{N^2} \sum'_{i, j} w_i^{k_1} w_j^{k_2} w_i^{k_3} w_j^{k_4} \langle \tilde{f}(u_i) \tilde{f}(u_j) \rangle^2 = - \frac{1}{NR^2} \langle uf(u) \rangle^4 \sum_{r, s} [S_{rs}^{k_1 k_3} S_{rs}^{k_2 k_4} - S_{rrss}^{k_1 k_3 k_2 k_4}], \quad (\text{A36})$$

which is again negligible in the large  $N$  limit.

*b. Three distinct indices* Let us study the contributions to the fourth moment of  $\lambda$  coming from three distinct indices. We study the case where  $i_1 = i_4$ :

$$E^{k_1 k_2 k_3 k_4} = \frac{1}{N^2} \sum'_{i_1, i_2, i_3} w_{i_1}^{k_1} w_{i_2}^{k_2} w_{i_3}^{k_3} w_{i_1}^{k_4} \langle \tilde{f}(u_{i_1})^2 \tilde{f}(u_{i_2}) \tilde{f}(u_{i_3}) \rangle. \quad (\text{A37})$$

Using the expression for the third moment of functions of  $u_1, u_2, u_3$  found in (A21), we get:

$$\begin{aligned} E^{k_1 k_2 k_3 k_4} &= cb^2 \frac{1}{N^2} \sum'_{i_1, i_2, i_3} w_{i_1}^{k_1} w_{i_2}^{k_2} w_{i_3}^{k_3} w_{i_1}^{k_4} - \text{Corr.} \\ &= cb^2 W^{k_1 k_4} [\Sigma^{k_2 k_3} - W^{k_2 k_3}] - \text{Corr.} \end{aligned} \quad (\text{A38})$$

The corrections come from cases when  $i_1 = i_2$  or  $i_1 = i_3$ . For instance the piece with  $i_1 = i_2$  gives

$$-cb^2 \frac{1}{ND} \sum_r S_r^{k_1 k_2 k_4} S_r^{k_3} \quad (\text{A39})$$

which is  $\mathcal{O}(1/N)$  at most.

The only pieces that do not vanish in the large  $N$  limit are thus the pieces similar to the one computed in (A38). Putting all of them together we find that the contribution to  $\langle \tilde{\lambda}^{k_1} \tilde{\lambda}^{k_2} \tilde{\lambda}^{k_3} \tilde{\lambda}^{k_4} \rangle$  coming from pieces with exactly three distinct indices in  $i_1, i_2, i_3, i_4$  is equal to:

$$G_3^{k_1 k_2 k_3 k_4} = cb^2 (X^{k_1 k_2; k_3 k_4} + X^{k_1 k_3; k_2 k_4} + X^{k_1 k_4; k_2 k_3} + X^{k_2 k_3; k_1 k_4} + X^{k_2 k_4; k_1 k_3} + X^{k_3 k_4; k_1 k_2})$$

where

$$X^{k_1 k_2; k_3 k_4} = W^{k_1 k_2} [\Sigma^{k_3 k_4} - W^{k_3 k_4}]. \quad (\text{A40})$$

*c. Two distinct indices* Let us now study the contribution to the fourth moment of  $\lambda$  coming from two distinct indices. We study first one piece of this contribution to the fourth moment, corresponding to  $i_1 = i_2 = i, i_3 = i_4 = j$ :

$$F^{k_1 k_2 k_3 k_4} = \frac{1}{N^2} \sum'_{i, j} w_i^{k_1} w_i^{k_2} w_j^{k_3} w_j^{k_4} \langle \tilde{f}(u_i)^2 \tilde{f}(u_j)^2 \rangle. \quad (\text{A41})$$

To leading order in the thermodynamic limit, we can write

$$\langle \tilde{f}(u_i)^2 \tilde{f}(u_j)^2 \rangle = c^2 \quad (\text{A42})$$

and therefore

$$F^{k_1 k_2 k_3 k_4} = c^2 W^{k_1 k_2} W^{k_3 k_4} \quad (\text{A43})$$

(the correction coming from  $i = j$  being obviously at most  $\mathcal{O}(1/N)$ ).

We study now the second piece of this contribution to the fourth moment, corresponding to  $i_1 = i_2 = i_3 = i, i_4 = j$ . This is equal to

$$\frac{1}{N^2} \sum'_{i, j} w_i^{k_1} w_i^{k_2} w_i^{k_3} w_j^{k_4} \langle \tilde{f}(u_i)^3 \tilde{f}(u_j) \rangle. \quad (\text{A44})$$

Using

$$\langle \tilde{f}(u_i)^3 \tilde{f}(u_j) \rangle = b \langle u \tilde{f}(u)^3 \rangle \frac{1}{D} \sum_r F_{ir} F_{jr}, \quad (\text{A45})$$

this gives

$$b \langle u \tilde{f}(u)^3 \rangle \frac{1}{ND} \sum_r S_r^{k_1 k_2 k_3} S_r^{k_4} \quad (\text{A46})$$

and it is therefore negligible.

Therefore all the contributions to the fourth moment of  $\lambda$  coming from exactly two distinct indices are of the type (A43). They give a total contribution:

$$G_2^{k_1 k_2 k_3 k_4} = c^2 [W^{k_1 k_2} W^{k_3 k_4} + W^{k_1 k_3} W^{k_2 k_4} + W^{k_1 k_4} W^{k_2 k_3}]. \quad (\text{A47})$$

*d. One distinct index* The contribution to the fourth moment  $\langle \lambda^{k_1} \lambda^{k_2} \lambda^{k_3} \lambda^{k_4} \rangle$  coming from  $i_1 = i_2 = i_3 = i_4$  is clearly of  $\mathcal{O}(1/N)$  and can be neglected.

*e. Final result for the four-point correlation function of  $\lambda$  variables* We can now put together all the contributions to the fourth moment  $\langle \tilde{\lambda}^{k_1} \tilde{\lambda}^{k_2} \tilde{\lambda}^{k_3} \tilde{\lambda}^{k_4} \rangle$  coming from pieces with four distinct indices found in (A32), those with three distinct indices found in (A40), and those with two distinct indices found in (A47). Defining

$$Y^{k_1 k_2} = \Sigma^{k_1 k_2} - W^{k_1 k_2}, \quad (\text{A48})$$

and recalling the definition (A40) of the  $X$  variables, we obtain:

$$\begin{aligned} \langle \tilde{\lambda}^{k_1} \tilde{\lambda}^{k_2} \tilde{\lambda}^{k_3} \tilde{\lambda}^{k_4} \rangle &= b^4 (Y^{k_1 k_2} Y^{k_3 k_4} + Y^{k_1 k_3} Y^{k_2 k_4} + Y^{k_1 k_4} Y^{k_2 k_3}) \\ &\quad + b^2 c (X^{k_1 k_2; k_3 k_4} + X^{k_1 k_3; k_2 k_4} \\ &\quad + X^{k_1 k_4; k_2 k_3} + X^{k_2 k_3; k_1 k_4} + X^{k_2 k_4; k_1 k_3} + X^{k_3 k_4; k_1 k_2}) \\ &\quad + c^2 [W^{k_1 k_2} W^{k_3 k_4} + W^{k_1 k_3} W^{k_2 k_4} + W^{k_1 k_4} W^{k_2 k_3}]. \end{aligned} \quad (\text{A49})$$

We can see that this is equal to

$$[b^2 Y^{k_1 k_2} + c W^{k_1 k_2}] [b^2 Y^{k_3 k_4} + c W^{k_3 k_4}] + 2 \text{ perm.} \quad (\text{A50})$$

which shows that

$$\langle \tilde{\lambda}^{k_1} \tilde{\lambda}^{k_2} \tilde{\lambda}^{k_3} \tilde{\lambda}^{k_4} \rangle = \langle \tilde{\lambda}^{k_1} \tilde{\lambda}^{k_2} \rangle \langle \tilde{\lambda}^{k_3} \tilde{\lambda}^{k_4} \rangle + 2 \text{ permutations.} \quad (\text{A51})$$

With this, it is clear how to proceed with the calculation of the fourth moments involving  $\lambda$  and  $\nu$  variables. We first need to study the moments with three  $\lambda$  and one  $\nu$ , then moments with two  $\lambda$  and two  $\nu$ , and finally the moments with one  $\lambda$  and three  $\nu$  variables. In the interest of conciseness, we do not spell out the full details of this calculations here, which proceeds very similarly to the calculations performed hitherto.

The generalisation to higher moments of  $\lambda$  variables employs the same combination of repeated use of Lemma A.2 and careful decomposition in subsets of distinct indices. As a result, it can be seen that the set of  $\lambda$  variables has a Gaussian distribution in the thermodynamic limit.

## Appendix B: Derivation of the equations of motion

When we make a step of SGD, we update the weight  $w_i^k$  using a new sample, generated using a previously unused sample according to

$$(w_i^k)_{\mu+1} - (w_i^k)_\mu = -\frac{\eta}{\sqrt{N}} v^k \Delta g'(\lambda^k) f(u_i), \quad (\text{B1a})$$

$$v_{\mu+1}^k - v_\mu^k = -\frac{\eta}{N} g(\lambda^k) \Delta, \quad (\text{B1b})$$

where  $\Delta = \sum_{j=1}^K v^j g(\lambda^j) - \sum_{m=1}^M \tilde{v}^m \tilde{g}(\nu^m)$ . Note the different re-scaling of the learning rate for the first and second-layer weights. From here on out, we shall drop the index  $\mu$  on the right-hand side as we work at a fixed iteration time. We will keep the convention of Sec. III A where extensive indices (taking values up to  $N$  or  $D$ ) are below the line, while we'll use upper indices when they take finite values up to  $M$  or  $K$ . The challenge of controlling the learning in the thermodynamic limit will be to write closed equations using matrices with only ‘‘upper’’ indices left. Furthermore, we will adopt the convention that the indices  $j, k, \ell, \iota = 1, \dots, K$  always denote *student* nodes, while  $n, m = 1, \dots, M$  are reserved for teacher hidden nodes.

### 1. First steps

We will start by focussing on the dynamics of the first layer, Eq. (B1a). When we study the evolution of quantities that are linear in the weights, like  $S_r^k$  and the order parameters constructed from it, *e.g.*  $\Sigma^{k\ell}$ , we need to study

$$\left[ \sum_{j=1}^K v^j g(\lambda^j) - \sum_{m=1}^M \tilde{v}^m \tilde{g}(\nu^m) \right] g'(\lambda^k) f(u_i) = \sum_{j \neq k}^K v^j a_i^{jk} + v^k b_i^k - \sum_{n=1}^M \tilde{v}^n c_i^{nk}, \quad (\text{B2})$$

where

$$a_i^{jk} = g(\lambda^j)g'(\lambda^k)f(u_i), \quad (\text{B3})$$

$$b_i^k = g(\lambda^k)g'(\lambda^k)f(u_i), \quad (\text{B4})$$

$$c_i^{nk} = \tilde{g}(\nu^n)g'(\lambda^k)f(u_i). \quad (\text{B5})$$

while we keep the second-layer weights  $v^k$  fixed. We can thus follow the dynamics of  $S_r^k$  (20), which is linear in the weights and enters the definition of the order parameters  $R^{km}$  (17) and  $\Sigma^{kl}$  (22):

$$(S_r^k)_{\mu+1} - (S_r^k)_\mu = -\frac{\eta}{N}v^k \sum_i F_{ir} \left[ \sum_{j \neq k}^K v^j a_i^{jk} + v^k b_i^k - \sum_n^M \tilde{v}^n c_i^{nk} \right]. \quad (\text{B6})$$

We want to average this update equation over a new incoming sample, i.e. over the  $\mathbf{c}_r$  variables. Upon contraction with  $F_{ir}$  in Eq. (B6), we are thus led to computing the averages

$$\mathcal{A}_r^{jk} \equiv \frac{1}{\sqrt{N}} \sum_i \mathbb{E} [F_{ir} a_i^{jk}] = \mathbb{E} [g(\lambda^j)g'(\lambda^k)\beta_r], \quad (\text{B7})$$

$$\mathcal{B}_r^k \equiv \mathbb{E} [g(\lambda^k)g'(\lambda^k)\beta_r], \quad (\text{B8})$$

and

$$\mathcal{C}_r^{nk} = \mathbb{E} [\tilde{g}(\nu^n)g'(\lambda^k)\beta_r], \quad (\text{B9})$$

where

$$\beta_r = \frac{1}{\sqrt{N}} \sum_i F_{ir} f(u_i). \quad (\text{B10})$$

The crucial fact that allows for an analytic study of online learning is that, at each step  $\mu$  of SGD, a previously unseen input  $\mathbf{x}_\mu$  is used to evaluate the gradient. The latent representation  $\mathbf{c}_\mu$  of this input is given by a new set of i.i.d. Gaussian random variables  $c_{\mu r}$ , which are thus independent of the current weights of the student at that time. In the thermodynamic limit, the GEP of the previous section shows that, for one given value of  $r$ , the  $K + M + 1$  variables  $\{\lambda^k\}$ ,  $\{\nu^m\}$  and  $\beta_r$  have a joint Gaussian distribution, making it possible to express the averages over  $\{\lambda^k, \nu^m, \beta_r\}$  in terms of only their covariances.

Looking closer, we see that the average of (B7,B8,B9) over this Gaussian distribution involves two sets of random variables: on the one hand, the  $M + K$  local fields  $\{\nu^m, \lambda^k\}$ , which have correlations of order 1, and on the other hand the variable  $\beta_r$  (for one given value of  $r$ ). It turns out that  $\beta_r$  is only weakly correlated with the local fields  $\{\nu^m, \lambda^k\}$  (the correlation is  $\mathcal{O}(1/\sqrt{N})$ ). In Appendix A 1, we discuss how to compute this type of average and prove Lemma A.1, which for the averages (B7–B9) yields

$$\begin{aligned} \mathcal{A}_r^{jk} &= \frac{1}{Q^{kk}Q^{jj} - (Q^{kj})^2} (Q^{jj}\mathbb{E} [g'(\lambda^k)\lambda^k g(\lambda^j)] \mathbb{E} [\lambda^k \beta_r] - Q^{kj}\mathbb{E} [g'(\lambda^k)\lambda^j g(\lambda^j)] \mathbb{E} [\lambda^k \beta_r] \\ &\quad - Q^{kj}\mathbb{E} [g'(\lambda^k)\lambda^k g(\lambda^j)] \mathbb{E} [\lambda^j \beta_r] + Q^{kk}\mathbb{E} [g'(\lambda^k)\lambda^j g(\lambda^j)] \mathbb{E} [\lambda^j \beta_r]), \end{aligned} \quad (\text{B11})$$

$$\mathcal{B}_r^k = \frac{1}{Q^{kk}} \mathbb{E} [g'(\lambda^k)\lambda^k g(\lambda^k)] \mathbb{E} [\lambda^k \beta_r], \quad (\text{B12})$$

$$\begin{aligned} \mathcal{C}_r^{nk} &= \frac{1}{Q^{kk}T^{nn} - (R^{kn})^2} (T^{nn}\mathbb{E} [g'(\lambda^k)\lambda^k \tilde{g}(\nu^n)] \mathbb{E} [\lambda^k \beta_r] - R^{kn}\mathbb{E} [g'(\lambda^k)\nu^n \tilde{g}(\nu^n)] \mathbb{E} [\lambda^k \beta_r] \\ &\quad - R^{kn}\mathbb{E} [g'(\lambda^k)\lambda^k \tilde{g}(\nu^n)] \mathbb{E} [\nu^n \beta_r] + Q^{kk}\mathbb{E} [g'(\lambda^k)\nu^n \tilde{g}(\nu^n)] \mathbb{E} [\nu^n \beta_r]). \end{aligned} \quad (\text{B13})$$

This yields

$$(S_r^k)_{\mu+1} - (S_r^k)_\mu = -\frac{\eta}{\sqrt{N}}v^k \left[ \sum_{j \neq k}^K v^j \mathcal{A}_r^{jk} + v^k \mathcal{B}_r^k - \sum_n^M \tilde{v}^n \mathcal{C}_r^{nk} \right], \quad (\text{B14})$$

with only the single extensive index  $r$  left. While this equation would appear to open up a way to write down the equation of motion for the “teacher-student” overlap  $R^{km}$  by contracting (B14) with  $\tilde{w}_r^m$ , we show in Appendix C that such a program will lead to an infinite hierarchy of equations. To avoid this problem, we rotate the problem to a different basis, as we explain in the next section.

## 2. Changing the basis to close the equations

We can close the equations for the order parameters by studying their dynamics in the basis given by the eigenvectors of the operator

$$\Omega_{rs} \equiv \frac{1}{N} \sum_i F_{ir} F_{is}, \quad (\text{B15})$$

which is a  $D \times D$  symmetric matrix, with diagonal elements  $\Omega_{rr} = 1$ , and off-diagonal elements of order  $1/\sqrt{N}$ . Consider the orthogonal basis of eigenvectors  $\psi_{\tau=1,\dots,D}$  of this matrix, with corresponding eigenvalues  $\rho_\tau$ , such that

$$\sum_s \Omega_{rs} \psi_{\tau s} = \rho_\tau \psi_{\tau r}. \quad (\text{B16})$$

We will suppose that the components of the eigenvectors  $\psi_{\tau r}$  are of order 1 and we impose the following normalisation:

$$\sum_s \psi_{\tau s} \psi_{\tau' s} = D \delta_{\tau\tau'}, \quad \sum_\tau \psi_{\tau r} \psi_{\tau s} = D \delta_{rs}. \quad (\text{B17})$$

In this basis, the teacher-student overlap  $R^{km}$  (17) is given by

$$R^{km} = \frac{b}{D} \sum_\tau \Gamma_\tau^k \tilde{\omega}_\tau^m, \quad (\text{B18})$$

where we have introduced the projections

$$\Gamma_\tau^k = \frac{1}{\sqrt{D}} \sum_r S_r^k \psi_{\tau r} \quad (\text{B19})$$

and

$$\tilde{\omega}_\tau^m = \frac{1}{\sqrt{D}} \sum_r \tilde{w}_r^m \psi_{\tau r}. \quad (\text{B20})$$

Since  $\tilde{\omega}_\tau^m$  is a static variable, the time evolution of  $\Gamma_\tau^k$  is given by

$$(\Gamma_\tau^k)_{\mu+1} - (\Gamma_\tau^k)_\mu = -\frac{\eta}{\sqrt{\delta}N} v^k \sum_r \psi_{\tau r} \left[ \sum_{j \neq k}^K v^j \mathcal{A}_r^{jk} + v^k \mathcal{B}_r^k - \sum_n^M \tilde{v}^n \mathcal{C}_r^{nk} \right] \quad (\text{B21})$$

As we aim to compute the remaining sum over  $r$ , two types of terms appear:

$$\sum_r \psi_{\tau r} \mathbb{E} [\lambda^k \beta_r] = \frac{1}{\sqrt{\delta}} ((c - b^2)\delta + b^2 \rho_\tau) \Gamma_\tau^k = \frac{d_\tau}{\sqrt{\delta}} \Gamma_\tau^k, \quad (\text{B22})$$

where we have defined  $d_\tau = (c - b^2)\delta + b^2 \rho_\tau$ , and

$$\sum_r \psi_{\tau r} \mathbb{E} [\nu^n \beta_r] = \frac{b}{\sqrt{\delta}} \rho_\tau \tilde{\omega}_\tau^n. \quad (\text{B23})$$

Putting everything together, the final evolution of  $\Gamma_\tau^k$  is

$$\begin{aligned} (\Gamma_\tau^k)_{\mu+1} - (\Gamma_\tau^k)_\mu = & -\frac{\eta}{\delta N} v^k \left[ d_\tau \Gamma_\tau^k \sum_{j \neq k} v^j \frac{Q^{jj} \mathbb{E} [g'(\lambda^k) \lambda^k g(\lambda^j)] - Q^{kj} \mathbb{E} [g'(\lambda^k) \lambda^j g(\lambda^j)]}{Q^{kk} Q^{jj} - (Q^{kj})^2} \right. \\ & + \sum_{j \neq k} v^j d_\tau \Gamma_\tau^j \frac{Q^{kk} \mathbb{E} [g'(\lambda^k) \lambda^j g(\lambda^j)] - Q^{kj} \mathbb{E} [g'(\lambda^k) \lambda^k g(\lambda^j)]}{Q^{kk} Q^{jj} - (Q^{kj})^2} \\ & + d_\tau v^k \Gamma_\tau^k \frac{1}{Q^{kk}} \mathbb{E} [g'(\lambda^k) \lambda^k g(\lambda^k)] \\ & - d_\tau \Gamma_\tau^k \sum_n \tilde{v}^n \frac{T^{nn} \mathbb{E} [g'(\lambda^k) \lambda^k \tilde{g}(\nu^n)] - R^{kn} \mathbb{E} [g'(\lambda^k) \nu^n \tilde{g}(\nu^n)]}{Q^{kk} T^{nn} - (R^{kn})^2} \\ & \left. - b \rho_\tau \sum_n \tilde{v}^n \tilde{\omega}_\tau^n \frac{Q^{kk} \mathbb{E} [g'(\lambda^k) \nu^n \tilde{g}(\nu^n)] - R^{kn} \mathbb{E} [g'(\lambda^k) \lambda^k \tilde{g}(\nu^n)]}{Q^{kk} T^{nn} - (R^{kn})^2} \right]. \quad (\text{B24}) \end{aligned}$$

At this point, we note that the remaining averages appearing in this expression, such as  $\mathbb{E} [\lambda^k g'(\lambda^k) \tilde{g}(\nu^m)]$ , depend only on subsets of the local fields  $\{\lambda^{k=1,\dots,K}, \nu^{m=1,\dots,M}\}$ . As discussed above, the GEP guarantees that these random variables follow a multi-dimensional Gaussian distribution, so these averages depend only on the covariances of the local fields  $R^{km}$ ,  $Q^{k\ell}$ , and  $T^{mn}$ . To simplify the subsequent equations, we will use the shorthand notation for the three-dimensional Gaussian averages

$$I_3(k, j, n) \equiv \mathbb{E} [g'(\lambda^k) \lambda^j \tilde{g}(\nu^n)], \quad (\text{B25})$$

which was introduced by Saad & Solla [21] and that we discuss in the main text. To make this section self-contained, we recall that arguments passed to  $I_3$  should be translated into local fields on the right-hand side by using the convention where the indices  $j, k, \ell, \iota$  always refer to student local fields  $\lambda^j$ , etc., while the indices  $n, m$  always refer to teacher local fields  $\nu^n, \nu^m$ . Similarly,

$$I_3(k, j, j) \equiv \mathbb{E} [g'(\lambda^k) \lambda^j g(\lambda^j)], \quad (\text{B26})$$

where having the index  $j$  as the third argument means that the third factor is  $g(\lambda^j)$ , rather than  $\tilde{g}(\nu^m)$  in Eq. (B26). The average in Eq. (B26) is taken over a three-dimensional normal distribution with mean zero and covariance matrix

$$\Phi^{(3)}(k, j, n) = \begin{pmatrix} \mathbb{E} [\lambda^k \lambda^k] & \mathbb{E} [\lambda^k \lambda^j] & \mathbb{E} [\lambda^k \nu^n] \\ \mathbb{E} [\lambda^k \lambda^j] & \mathbb{E} [\lambda^j \lambda^j] & \mathbb{E} [\lambda^j \nu^n] \\ \mathbb{E} [\lambda^k \nu^n] & \mathbb{E} [\lambda^j \nu^n] & \mathbb{E} [\nu^n \nu^n] \end{pmatrix} = \begin{pmatrix} Q^{kk} & Q^{kj} & R^{kn} \\ Q^{kj} & Q^{jj} & R^{jn} \\ R^{kn} & R^{jn} & T^{nn} \end{pmatrix}. \quad (\text{B27})$$

### 3. Dynamics of the teacher-student overlap $R^{km}$

We are now in a position to write the update equation for

$$(R^{km})_{\mu+1} - (R^{km})_{\mu} = \frac{b}{D} \sum_{\tau} \left[ (\Gamma_{\tau}^k)_{\mu+1} - (\Gamma_{\tau}^k)_{\mu} \right] \tilde{\omega}_{\tau}^m, \quad (\text{B28})$$

where we have used that the  $\tilde{\omega}_{\tau}^m$  are static. When performing the last remaining sum over  $\tau$ , two types of terms appear. First, there is

$$\tilde{T}^{mn} \equiv \frac{1}{D} \sum_{\tau} \rho_{\tau} \tilde{\omega}_{\tau}^m \tilde{\omega}_{\tau}^n. \quad (\text{B29})$$

which depends only on the choice of the feature matrix  $F_{ir}$  and the teacher weights  $w_{mr}^*$  and is thus a constant of the motion. The second type of term is of the form

$$\frac{1}{D} \sum_{\tau} \rho_{\tau} \Gamma_{\tau}^{\ell} \tilde{\omega}_{\tau}^n. \quad (\text{B30})$$

This sum cannot be reduced to a simple expression in terms of other order parameters. Instead, we are led to introduce the density

$$r^{km}(\rho) = \frac{1}{\varepsilon_{\rho}} \frac{1}{D} \sum_{\tau} \Gamma_{\tau}^k \tilde{\omega}_{\tau}^m \mathbb{1}(\rho_{\tau} \in [\rho, \rho + \varepsilon_{\rho}]), \quad (\text{B31})$$

where  $\mathbb{1}(\cdot)$  is the indicator function which evaluates to 1 if the condition given to it as an argument is true, and which otherwise evaluates to 0. We take the limit  $\varepsilon_{\rho} \rightarrow 0$  after the thermodynamic limit. Then we can rewrite the order parameter  $R^{km}$  as an integral over the density  $r^{km}$ , weighted by the distribution of eigenvalues of the operator  $\Omega_{rs}$ ,  $p_{\Omega}(\rho)$ :

$$R^{km} = b \int d\rho p_{\Omega}(\rho) r^{km}(\rho). \quad (\text{B32})$$

If, for example, we take the elements of the feature matrix  $F_{ir}$  to be element-wise i.i.d. from the normal distribution with mean zero and unit variance, then the limiting density of eigenvalues of  $\Omega$  is given by the Marchenko-Pastur law [63]:

$$p_{\text{MP}}(\rho) = \frac{1}{2\pi\delta} \frac{\sqrt{(\rho_{\max} - \rho)(\rho - \rho_{\min})}}{\rho}, \quad (\text{B33})$$



where  $\rho_{\min} = (1 - \sqrt{\delta})^2$  and  $\rho_{\max} = (1 + \sqrt{\delta})^2$ .

The update equation of  $r^{km}(\rho)$  can be obtained immediately by substituting the update equation for  $\Gamma_\tau^k$  (B24) into its definition (B31). Finally, in the thermodynamic limit, the normalised number of steps  $t = P/N$  can be interpreted as a continuous time-like variable, and so we have

$$R^{km}(t) = b \int d\rho p_\Omega(\rho) r^{km}(\rho, t) \quad (\text{B34})$$

and we recover the equation of motion for  $r^{km}(\rho)$ , which we re-state here for ease of reading:

$$\begin{aligned} \frac{\partial r^{km}(\rho, t)}{\partial t} = & -\frac{\eta}{\delta} v^k \left( d(\rho) r^{km}(\rho) \sum_{j \neq k} v^j \frac{Q^{jj} I_3(k, k, j) - Q^{kj} I_3(k, j, j)}{Q^{jj} Q^{kk} - (Q^{kj})^2} \right. \\ & + d(\rho) \sum_{j \neq k} v^j r^{jm}(\rho) \frac{Q^{kk} I_3(k, j, j) - Q^{kj} I_3(k, k, j)}{Q^{jj} Q^{kk} - (Q^{kj})^2} \\ & + v^k d(\rho) r^{km}(\rho) \frac{1}{Q^{kk}} I_3(k, k, k) \\ & - d(\rho) r^{km}(\rho) \sum_n \tilde{v}^n \frac{T^{nn} I_3(k, k, n) - R^{kn} I_3(k, n, n)}{Q^{kk} T^{nn} - (R^{kn})^2} \\ & \left. - b\rho \sum_n \tilde{v}^n \tilde{T}^{nm} \frac{Q^{kk} I_3(k, n, n) - R^{kn} I_3(k, k, n)}{Q^{kk} T^{nn} - (R^{kn})^2} \right), \end{aligned} \quad (\text{B35})$$

where  $d(\rho) = (c - b^2)\delta + b^2\rho$ . Note that while we have dropped the explicit time dependence from the right-hand side to keep the equation readable, all the order parameters on the right-hand side are explicitly time-dependent, i.e.  $Q^{jj} = Q^{jj}(t)$ ,  $r^{km}(\rho) = r^{km}(\rho, t)$ , and the averages  $I_3(\cdot)$  are also time-dependent via their dependence on the order parameters (see Eq. (B26) and the subsequent discussion). In order to close the equations of motion, we now need to find the equations for the order parameters that are quadratic in the weights.

#### 4. Order parameters that are quadratic in the weights

There are two order parameters that appear when evaluating the covariance of the  $\lambda$  variables:

$$Q^{k\ell} \equiv \mathbb{E} [\lambda^k \lambda^\ell] = [c - b^2] W^{k\ell} + b^2 \Sigma^{k\ell}. \quad (\text{B36})$$

We will look at both  $W^{k\ell}$  and  $\Sigma^{k\ell}$  in turn now.

*a. Equation of motion for  $W^{k\ell}$*  For the student-student overlap matrix

$$W^{k\ell} = \frac{1}{N} \sum_i^N w_i^k w_i^\ell, \quad (\text{B37})$$

we find, after some algebra, that updates read

$$\begin{aligned} (W^{k\ell})^{\mu+1} - (W^{k\ell})_\mu = & -\frac{\eta}{N^{3/2}} v^k \sum_i^N w_i^\ell \left[ \sum_{j \neq k}^K v^j a_i^{jk} + v^k b_i^k - \sum_n^M \tilde{v}^n c_i^{nk} \right] \\ & - \frac{\eta}{N^{3/2}} v^\ell \sum_i^N w_i^k \left[ \sum_{j \neq \ell}^K v^j a_i^{j\ell} + v^\ell b_i^\ell - \sum_n^M \tilde{v}^n c_i^{n\ell} \right] \\ & + \frac{\eta^2}{N^2} v^k v^\ell \sum_i^N f(u_i)^2 g'(\lambda^k) g'(\lambda^\ell) \left[ \sum_{j, \iota}^K v^j v^\iota g(\lambda^j) g(\lambda^\iota) + \sum_{n, m}^M \tilde{v}^n \tilde{v}^m \tilde{g}(\nu^n) \tilde{g}(\nu^m) \right. \\ & \left. - 2 \sum_j^K \sum_m^M v^j \tilde{v}^m g(\lambda^j) \tilde{g}(\nu^m) \right] \end{aligned} \quad (\text{B38})$$

For the terms linear in the learning rate  $\eta$ , we can immediately carry out the sum over  $i$ , which yields terms of the type

$$\frac{1}{\sqrt{N}} \sum_i w_i^\ell \mathbb{E} [g(\lambda^j) g'(\lambda^k) f(u_i)] = \mathbb{E} [g'(\lambda^k) \lambda^\ell g(\lambda^j)] = I_3(k, \ell, j) \quad \text{etc.} \quad (\text{B39})$$

The term quadratic in the learning rate  $\eta$  requires the evaluation of terms of the type

$$\frac{1}{N} \sum_i \mathbb{E} [f(u_i)^2 g'(\lambda^k) g'(\lambda^\ell) g(\lambda^j) g(\lambda^\iota)] = c \mathbb{E} [g'(\lambda^k) g'(\lambda^\ell) g(\lambda^j) g(\lambda^\iota)]. \quad (\text{B40})$$

The sum over  $i$  thus makes this second-order term contribute to the total variation of  $W^{k\ell}$  at leading order, and we're left with an average over four local fields, for which we introduce the short-hand

$$I_4(k, \ell, j, \iota) \equiv \mathbb{E} [g'(\lambda^k) g'(\lambda^\ell) g(\lambda^j) g(\lambda^\iota)], \quad (\text{B41})$$

where we use the same notation as we did for  $I_3(\cdot)$  (B26). The full equation of motion for  $W^{k\ell}$  thus reads

$$\begin{aligned} \frac{dW^{k\ell}(t)}{dt} = & -\eta v^k \left( \sum_j^K v^j I_3(k, \ell, j) - \sum_n \tilde{v}^n I_3(k, \ell, n) \right) - \eta v^\ell \left( \sum_j^K v^j I_3(\ell, k, j) - \sum_n \tilde{v}^n I_3(\ell, k, n) \right) \\ & + c \eta^2 v^k v^\ell \left( \sum_{j,a}^K v^j v^a I_4(k, \ell, j, a) - 2 \sum_j^K \sum_m^M v^j \tilde{v}^m I_4(k, \ell, j, m) + \sum_{n,m}^M \tilde{v}^n \tilde{v}^m I_4(k, \ell, n, m) \right). \end{aligned} \quad (\text{B42})$$

*b. Equation of motion for  $\Sigma^{k\ell}$*  After rotating to the basis  $\psi_\tau$ , we have

$$\Sigma^{k\ell} \equiv \frac{1}{D} \sum_r S_r^k S_r^\ell = \frac{1}{D} \sum_\tau \Gamma_\tau^k \Gamma_\tau^\ell. \quad (\text{B43})$$

It is then immediate that

$$\begin{aligned} (\Sigma^{k\ell})^{\mu+1} - (\Sigma^{k\ell})_\mu &= \frac{1}{D} \sum_\tau (\Gamma_\tau^\ell)_\mu \left[ (\Gamma_\tau^k)^{\mu+1} - (\Gamma_\tau^k)_\mu \right] + \frac{1}{D} \sum_\tau (\Gamma_\tau^k)_\mu \left[ (\Gamma_\tau^\ell)^{\mu+1} - (\Gamma_\tau^\ell)_\mu \right] \\ &+ \frac{\eta^2}{D^2 N} \sum_\tau \sum_{r,s}^R \psi_{\tau r} \psi_{\tau s} \mathbb{E} [\Delta^2 g'(\lambda^k) g'(\lambda^\ell) \beta_r \beta_s]. \end{aligned} \quad (\text{B44})$$

The terms linear in  $\eta$  can be obtained directly by substituting in the update equation for  $\Gamma_\tau^k$  (B24) and are similar to the update equation for  $r^{km}(\rho)$ . As for the term quadratic in  $\eta$ , we have to leading order

$$\begin{aligned} \frac{\eta^2}{DN} \sum_{r,s}^R \psi_{\tau r} \psi_{\tau s} \mathbb{E} [\Delta^2 g'(\lambda^k) g'(\lambda^\ell) \beta_r \beta_s] &= \frac{\eta^2}{DN} \sum_r^R (\psi_{\tau r})^2 \mathbb{E} [\Delta^2 g'(\lambda^k) g'(\lambda^\ell)] \mathbb{E} [\beta_r^2] \\ &= \frac{\eta^2}{N} \mathbb{E} [\Delta^2 g'(\lambda^k) g'(\lambda^\ell)] \left[ (c - b^2) \rho_\tau + \frac{b^2}{\delta} \rho_\tau^2 \right], \end{aligned} \quad (\text{B45})$$

where we have used that covariance of  $\beta_r$  is given by

$$\mathbb{E} [\beta_r^2] = c - b^2 + \frac{b^2}{\delta} \sum_t \Omega_{rt}^2. \quad (\text{B46})$$

To deal with the remaining sum over  $\tau$ , we again make use of the fact that the equation of motion for  $\Sigma^{k\ell}$  depends on the eigenvector index  $\tau$  only through the eigenvalue  $\rho_\tau$ . Introducing the density

$$\sigma^{k\ell}(\rho) = \frac{1}{\varepsilon_\rho} \frac{1}{D} \sum_\tau \Gamma_\tau^k \Gamma_\tau^\ell \mathbb{1}(\rho_\tau \in [\rho, \rho + \varepsilon_\rho]), \quad (\text{B47})$$

as we did for  $r^{km}(\rho)$  (B31), we have

$$\Sigma^{k\ell}(t) = \int d\rho p_\Omega(\rho) \sigma^{k\ell}(\rho, t) \quad (\text{B48})$$

with

$$\begin{aligned} \frac{\partial \sigma^{k\ell}(\rho, t)}{\partial t} = & -\frac{\eta}{\delta} \left( d(\rho) v^k \sigma^{k\ell}(\rho) \sum_{j \neq k} v^j \frac{Q^{jj} I_3(k, k, j) - Q^{kj} I_3(k, j, j)}{Q^{jj} Q^{kk} - (Q^{kj})^2} \right. \\ & + v^k \sum_{j \neq k} v^j d(\rho) \sigma^{j\ell}(\rho) \frac{Q^{kk} I_3(k, j, j) - Q^{kj} I_3(k, k, j)}{Q^{jj} Q^{kk} - (Q^{kj})^2} \\ & + d(\rho) v^k \sigma^{k\ell}(\rho) v^k \frac{1}{Q^{kk}} I_3(k, k, k) \\ & - d(\rho) v^k \sigma^{k\ell}(\rho) \sum_n \tilde{v}^n \frac{T^{nn} I_3(k, k, n) - R^{kn} I_3(k, n, n)}{Q^{kk} T^{nn} - (R^{kn})^2} \\ & - b\rho v^k \sum_n \tilde{v}^n r^{\ell n}(\rho) \frac{Q^{kk} I_3(k, n, n) - R^{kn} I_3(k, k, n)}{Q^{kk} T^{nn} - (R^{kn})^2} \\ & \left. + \text{all of the above with } \ell \rightarrow k, k \rightarrow \ell \right) \\ & + \eta^2 v^k v^\ell \left[ (c - b^2)\rho + \frac{b^2}{\delta} \rho^2 \right] \left( \sum_{j, \ell} v^j v^\ell I_4(k, \ell, j, \ell) \right. \\ & \left. - 2 \sum_j \sum_m v^j \tilde{v}^m I_4(k, \ell, j, m) + \sum_{n, m} \tilde{v}^n \tilde{v}^m I_4(k, \ell, n, m) \right) \end{aligned} \quad (\text{B49})$$

## 5. Second-layer weights

Finally, we will treat each of the second-layer weights of the student  $\mathbf{v}$  as an order parameter in its own right. Their equations of motion are readily found from their SGD update (B1b), and read

$$\frac{dv^k}{dt} = \eta \left[ \sum_n \tilde{v}_n I_2(k, n) - \sum_j v^j I_2(k, j) \right], \quad (\text{B50})$$

where we have introduced the final short-hand

$$I_2(k, j) \equiv \mathbb{E} [g(\lambda^k) g(\lambda^j)] \text{ etc.} \quad (\text{B51})$$

where we again use the notation we introduced for  $I_3(\cdot)$  (B26).

## 6. Summary of the derivation

We have now completed the programme that we embarked upon at the beginning of this Appendix B: we have derived a closed set of equations of motion for the teacher-student overlap  $R^{km}$  (B32,29) the student-student overlap  $Q^{k\ell} = [c - b^2] W^{k\ell} + b^2 \Sigma^{k\ell}$  (38,34,35), and the student's second-layer weights  $v^k$  (39). These equations give us complete access to the dynamics of a neural network performing one-shot stochastic gradient descent on a data set generated by the hidden manifold model. We can now integrate these equations and substitute the values of the order parameters at any time into the expression for the generalisation error (25), thereby tracking the dynamics of the generalisation error at all times. We describe this procedure in more detail next.

### 7. Explicit form of the integrals $I_3$ and $I_4$ for sigmoidal students

The explicit forms of the integrals  $I_3$  and  $I_4$  that appear in the equations of motion for the order parameters and the generalisation error for networks with  $g(x) = \tilde{g}(x) = \text{erf}(x/\sqrt{2})$  were first given by [20, 21]. Here, we will state them to make the paper as self-contained as possible. Denoting the elements of the covariance matrix such as  $\Phi^3$  (B27) as  $\phi_{ij}$ , we have

$$I_3(\cdot, \cdot, \cdot) = \frac{2}{\pi} \frac{1}{\sqrt{\Lambda_3}} \frac{\phi_{23}(1 + \phi_{11}) - \phi_{12}\phi_{13}}{1 + \phi_{11}} \quad (\text{B52})$$

with

$$\Lambda_3 = (1 + \phi_{11})(1 + \phi_{33}) - \phi_{13}^2. \quad (\text{B53})$$

For the average  $I_4$ , we have a covariance matrix  $\Phi^{(4)}$  that is populated in analogy to  $\Phi^{(3)}$  (B27), we have

$$I_4(\cdot, \cdot, \cdot) = \frac{4}{\pi^2} \frac{1}{\sqrt{\Lambda_4}} \arcsin\left(\frac{\Lambda_0}{\sqrt{\Lambda_1\Lambda_2}}\right) \quad (\text{B54})$$

where

$$\Lambda_4 = (1 + \phi_{11})(1 + \phi_{22}) - \phi_{12}^2, \quad (\text{B55})$$

$$\Lambda_0 = \Lambda_4\phi_{34} - \phi_{23}\phi_{24}(1 + \phi_{11}) - \phi_{13}\phi_{14}(1 + \phi_{22}) + \phi_{12}\phi_{13}\phi_{24} + \phi_{12}\phi_{14}\phi_{23}, \quad (\text{B56})$$

$$\Lambda_1 = \Lambda_4(1 + \phi_{33}) - \phi_{23}^2(1 + \phi_{11}) - \phi_{13}^2(1 + \phi_{22}) + 2\phi_{12}\phi_{13}\phi_{23}, \quad (\text{B57})$$

$$\Lambda_2 = \Lambda_4(1 + \phi_{44}) - \phi_{24}^2(1 + \phi_{11}) - \phi_{14}^2(1 + \phi_{22}) + 2\phi_{12}\phi_{14}\phi_{24} \quad (\text{B58})$$

### Appendix C: The equations of motion do not close in the trivial basis

Here we give a short demonstration that it is not possible to close the equations for order parameters if we do not rotate their dynamics to the basis given by the eigenvectors of  $\Omega$ , which is what we do in our derivation in Sec. III B.

#### 1. Order parameters that are linear in the weights

To start with a variable that is linear in the weights, take the time-evolution of  $S_r^k$ . It is clear that the tensor structure of the result (B14) will be of the form

$$(S_r^k)^{\mu+1} - (S_r^k)^\mu = -\frac{\eta}{N} \left[ \sum_\ell D^{k\ell} \sum_s \Omega_{rs} S_s^\ell + \sum_m E^{km} \sum_s \Omega_{rs} \tilde{w}_s^m \right] \quad (\text{C1})$$

where  $D^{k\ell}$  and  $E^{km}$  are known quantities, expressed in terms of the matrices  $Q, T, R$ , and we have introduced the operator

$$\Omega_{rs} = \frac{1}{N} \sum_i F_{ir} F_{is} \quad (\text{C2})$$

which has diagonal elements equal 1, and off diagonal elements of order  $1/\sqrt{N}$ .

In particular we can use this evolution to study the evolution of  $R$ :

$$(R^{km})^{\mu+1} - (R^{km})^\mu = -\langle uf(u) \rangle \frac{\eta}{N} \left[ \sum_\ell D^{k\ell} \frac{1}{D} \sum_{rs} \tilde{w}_r^m \Omega_{rs} S_s^\ell + \sum_m E^{km} \frac{1}{D} \sum_{rs} \tilde{w}_s^r \Omega_{rs} \tilde{w}_s^m \right] \quad (\text{C3})$$

The point of this analysis is to show that the time evolution of  $S_r^k$  involves  $(\Omega S)_r^\ell$ . Therefore to know the evolution of  $S$  we need the one of  $\Omega S$ . This is not innocuous because, in order to have dynamical evolution equations with only ‘‘up’’ indices, we need to contract it. The evolution of  $R^{km}$ , which is proportional to the scalar product (in the  $R$ -dimensional manifold space) of  $S^k$  and  $\tilde{w}^m$ , is thus given by the scalar product of  $\Omega S^k$  and  $\tilde{w}^m$ .

It is not difficult to see that the evolution of  $\Omega S$  will require knowing  $\Omega^2 S$  etc. So we have an infinite hierarchy of coupled equations. However, these can be closed by changing basis for  $S$ .

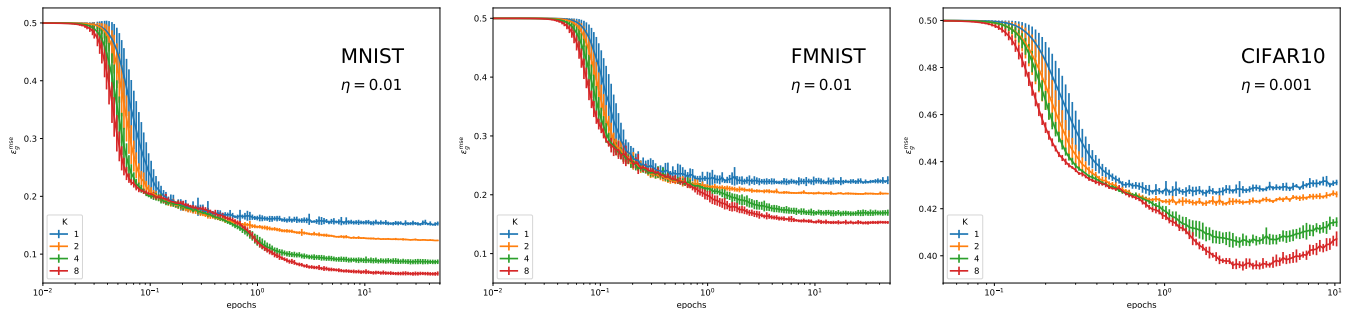


FIG. 10. **Two-layer sigmoidal neural networks learn functions of increasing complexity on different data sets.** We plot the mean-squared error as a function of training time for sigmoidal networks with increasing hidden layer when trained on three different data sets. The curves are obtained by averaging ten different runs, starting from different initial weights. Error bars indicate one standard deviation. For all plots,  $g(x) = \text{erf}(x/\sqrt{2})$ , gaussian initial weights with std. dev.  $10^{-3}$ , batch size 32.

#### Appendix D: Additional details on the numerical experiments in Sec. V A

For the experiments demonstrating the learning of functions of increasing complexity discussed in Sec. V A, we constructed data sets for binary classification by splitting the image data sets as follows:

**MNIST:** even vs. odd numbers

**Fashion MNIST:** t-shirt/top, pullover, dress, sandal and bag vs. trouser, coat, shirt, sneaker, ankle boot

**CIFAR10:** air plane, bird, deer, frog, ship vs. automobile, cat, dog, horse and truck.

We first demonstrate in Fig. 10 that sigmoidal networks show the same learning of functions of increasing complexity discussed in Sec. V A for CIFAR10 when trained on MNIST or FMNIST. Note that for CIFAR10 in particular, we see the effects of over-training set in after several epochs, when the generalisation error starts to increase again (we use plain SGD without any explicit regularisation in these experiments).

We also repeated these experiments for ReLU networks with activation function  $g(x) = \max(0, x)$ . While the dynamics of ReLU students also show a progression from simple to more complex classifiers, the run-to-run fluctuations are much larger than for the sigmoidal students. This is true both quantitatively, but also qualitatively: for example, networks sometimes get stuck in really sub-optimal minimisers for a long time. Hence, plotting the mean trajectories is not as informative as the standard variations would be very high, so in Fig. 11 we instead show representative curves for individual runs of ReLU students for all three data sets and for online learning from a teacher with  $\tilde{g}(x) = \max(x, 0)$ ,  $M = 10$ ,  $\tilde{v}^m = 1/M$ .

- 
- [1] A. Krizhevsky, I. Sutskever, and G.E. Hinton, “Imagenet classification with deep convolutional neural networks,” in *Advances in neural information processing systems* (2012) pp. 1097–1105.
  - [2] Y. LeCun, Y. Bengio, and G.E. Hinton, “Deep learning,” *Nature* **521**, 436–444 (2015).
  - [3] I. Sutskever, O. Vinyals, and Q.V. Le, “Sequence to sequence learning with neural networks,” in *Advances in Neural Information Processing Systems 27*, edited by Z. Ghahramani, M. Welling, C. Cortes, N. D. Lawrence, and K. Q. Weinberger (Curran Associates, Inc., 2014) pp. 3104–3112.
  - [4] V. Vapnik, *The nature of statistical learning theory* (Springer science & business media, 2013).
  - [5] M. Mohri, A. Rostamizadeh, and A. Talwalkar, *Foundations of Machine Learning* (MIT Press, 2012).
  - [6] E. Gardner and B. Derrida, “Three unfinished works on the optimal storage capacity of networks,” *Journal of Physics A: Mathematical and General* **22**, 1983–1994 (1989).
  - [7] H. S. Seung, H. Sompolinsky, and N. Tishby, “Statistical mechanics of learning from examples,” *Physical Review A* **45**, 6056–6091 (1992).
  - [8] A. Engel and C. Van den Broeck, *Statistical Mechanics of Learning* (Cambridge University Press, 2001).
  - [9] L. Zdeborová and F. Krzakala, “Statistical physics of in-

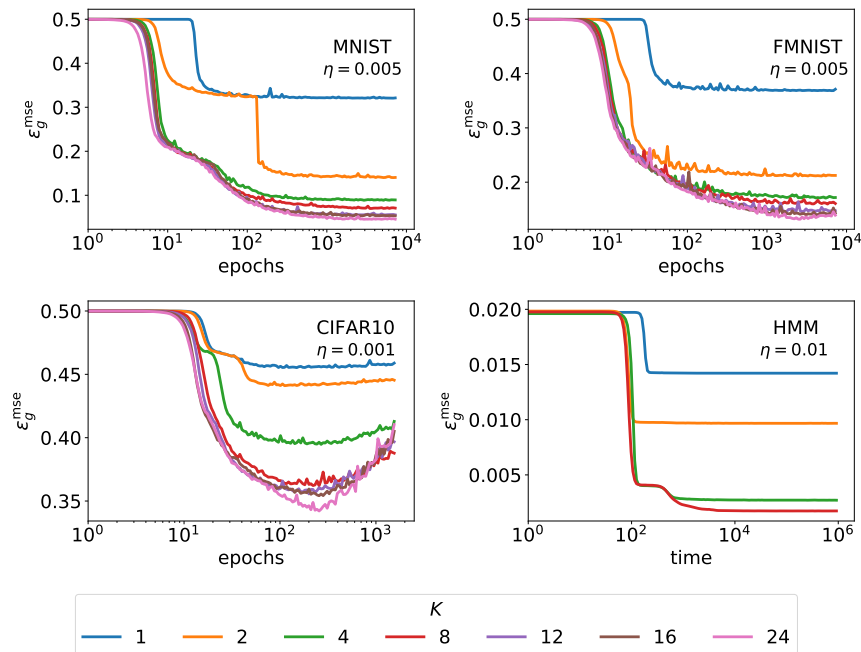


FIG. 11. **Two-layer ReLU neural networks also learn functions of increasing complexity, show more run-to-run variance.** We plot the mean-squared error as a function of training time for sigmoidal networks with increasing number of nodes  $K$  when trained on three different data sets. For all plots,  $g(x) = \max(0, x)$ , gaussian initial weights with std. dev.  $10^{-3}$ , batch size 32. For online learning, we chose a teacher with  $\tilde{g}(x) = \max(x, 0)$ ,  $M = 10$ ,  $\tilde{v}^m = 1/M$ .

- ference: thresholds and algorithms,” *Adv. Phys.* **65**, 453–552 (2016).
- [10] Y. LeCun and C. Cortes, “The MNIST database of handwritten digits,” (1998).
- [11] Alex Krizhevsky, Geoffrey Hinton, *et al.*, “Learning multiple layers of features from tiny images,” (2009).
- [12] P. Grassberger and I. Procaccia, “Measuring the strangeness of strange attractors,” *Physica D: Nonlinear Phenomena* **9**, 189–208 (1983).
- [13] J.A. Costa and A.O. Hero, “Learning intrinsic dimension and intrinsic entropy of high-dimensional datasets,” in *2004 12th European Signal Processing Conference* (2004) pp. 369–372.
- [14] E. Levina and P.J. Bickel, “Maximum likelihood estimation of intrinsic dimension,” in *Advances in Neural Information Processing Systems 17* (2004).
- [15] S. Spigler, M. Geiger, and M. Wyart, “Asymptotic learning curves of kernel methods: empirical data v.s. Teacher-Student paradigm,” preprint (2019), arXiv:1905.10843.
- [16] I. Goodfellow, J. Pouget-Abadie, M. Mirza, B. Xu, D. Warde-Farley, S. Ozair, A. Courville, and Y. Bengio, “Generative adversarial nets,” in *Advances in neural information processing systems* (2014) pp. 2672–2680.
- [17] A. Radford, L. Metz, and S. Chintala, “Unsupervised representation learning with deep convolutional generative adversarial networks,” (2015), arXiv:1511.06434.
- [18] T. Karras, S. Laine, M. Aittala, J. Hellsten, J. Lehtinen, and T. Aila, “Analyzing and improving the image quality of stylegan,” (2019), arXiv:1912.04958.
- [19] W. Kinzel and P. Ruján, “Improving a Network Generalization Ability by Selecting Examples,” *EPL (Europhysics Letters)* **13**, 473–477 (1990).
- [20] M. Biehl and H. Schwarze, “Learning by on-line gradient descent,” *J. Phys. A: Math. Gen.* **28**, 643–656 (1995).
- [21] D. Saad and S.A. Solla, “Exact Solution for On-Line Learning in Multilayer Neural Networks,” *Phys. Rev. Lett.* **74**, 4337–4340 (1995).
- [22] H. Xiao, K. Rasul, and R. Vollgraf, “Fashion-mnist: a novel image dataset for benchmarking machine learning algorithms,” (2017), arXiv:1708.07747.
- [23] J. Bruna and S. Mallat, “Invariant scattering convolution networks,” *IEEE transactions on pattern analysis and machine intelligence* **35**, 1872–1886 (2013).
- [24] A.B. Patel, M.T. Nguyen, and R. Baraniuk, “A probabilistic framework for deep learning,” in *Advances in Neural Information Processing Systems 29*, edited by D. D. Lee, M. Sugiyama, U. V. Luxburg, I. Guyon, and R. Garnett (Curran Associates, Inc., 2016) pp. 2558–2566.
- [25] M. Mézard, “Mean-field message-passing equations in the hopfield model and its generalizations,” *Physical Review E* **95**, 022117 (2017).
- [26] M. Gabrié, A. Manoel, C. Luneau, J. Barbier, N. Macris, F. Krzakala, and L. Zdeborová, “Entropy and mutual information in models of deep neural networks,” in *Advances in Neural Information Processing Systems 31* (2018) pp. 1826–1836.
- [27] E. Mossel, “Deep learning and hierarchical generative models,” (2018), arXiv:1612.09057.
- [28] S. Chung, Daniel D. Lee, and H. Sompolinsky, “Classification and Geometry of General Perceptual Manifolds,” *Physical Review X* **8**, 31003 (2018).
- [29] SY Chung, U. Cohen, H. Sompolinsky, and D.D. Lee, “Learning data manifolds with a cutting plane method,” *Neural computation* **30**, 2593–2615 (2018).

- [30] U. Cohen, SY Chung, D.D. Lee, and H. Sompolinsky, “Separability and geometry of object manifolds in deep neural networks,” *Nature communications* **11**, 1–13 (2020).
- [31] P. Rotondo, M. Cosentino Lagomarsino, and M. Gherardi, “Counting the learnable functions of structured data,” preprint (2019), arXiv:1903.12021.
- [32] T.M. Cover, “Geometrical and Statistical Properties of Systems of Linear Inequalities with Applications in Pattern Recognition,” *IEEE Transactions on Electronic Computers* **EC-14**, 326–334 (1965).
- [33] Y. Yoshida and M. Okada, “Data-dependence of plateau phenomenon in learning with neural network — statistical mechanical analysis,” in *Advances in Neural Information Processing Systems 32* (2019) pp. 1720–1728.
- [34] F. Rosenblatt, *Principles of Neurodynamics* (Spartan, 1962).
- [35] A. Rahimi and B. Recht, “Random features for large-scale kernel machines,” in *Advances in neural information processing systems* (2008) pp. 1177–1184.
- [36] A. Rahimi and B. Recht, “Weighted sums of random kitchen sinks: Replacing minimization with randomization in learning,” in *Advances in neural information processing systems* (2009) pp. 1313–1320.
- [37] C. Louart, Z. Liao, and Romain Couillet, “A random matrix approach to neural networks,” *The Annals of Applied Probability* **28**, 1190–1248 (2018).
- [38] S. Mei and A. Montanari, “The generalization error of random features regression: Precise asymptotics and double descent curve,” (2019), arXiv:1908.05355.
- [39] A. Montanari, F. Ruan, Y. Sohn, and J. Yan, “The generalization error of max-margin linear classifiers: High-dimensional asymptotics in the overparametrized regime,” (2019), arXiv:1911.01544.
- [40] W. Hachem, P. Loubaton, and J. Najim, “Deterministic equivalents for certain functionals of large random matrices,” *Ann. Appl. Probab.* **17**, 875–930 (2007).
- [41] X. Cheng and A. Singer, “The spectrum of random inner-product kernel matrices,” *Random Matrices: Theory and Applications* **2**, 1350010 (2013).
- [42] Z. Fan and A. Montanari, “The spectral norm of random inner-product kernel matrices,” *Probability Theory and Related Fields* **173**, 27–85 (2019).
- [43] J. Pennington and P. Worah, “Nonlinear random matrix theory for deep learning,” in *Advances in Neural Information Processing Systems* (2017) pp. 2637–2646.
- [44] M.E.A. Seddik, M. Tamaazousti, and R. Couillet, “Kernel random matrices of large concentrated data: the example of gan-generated images,” in *ICASSP 2019-2019 IEEE International Conference on Acoustics, Speech and Signal Processing (ICASSP)* (IEEE, 2019) pp. 7480–7484.
- [45] M.E.A. Seddik, C. Louart, M. Tamaazousti, and R. Couillet, “Random matrix theory proves that deep learning representations of gan-data behave as gaussian mixtures,” (2020), arXiv:2001.08370.
- [46] “An ODE integrator and source code for all experiments can be found at,” <https://github.com/sgoldt/hidden-manifold-model>.
- [47] T.L.H. Watkin, A. Rau, and M. Biehl, “The statistical mechanics of learning a rule,” *Reviews of Modern Physics* **65**, 499–556 (1993).
- [48] M.S. Advani and A.M. Saxe, “High-dimensional dynamics of generalization error in neural networks,” (2017), arXiv:1710.03667.
- [49] B. Aubin, A. Maillard, J. Barbier, F. Krzakala, N. Macris, and L. Zdeborová, “The committee machine: Computational to statistical gaps in learning a two-layers neural network,” in *Advances in Neural Information Processing Systems 31* (2018) pp. 3227–3238.
- [50] J. Barbier, F. Krzakala, N. Macris, L. Miolane, and L. Zdeborová, “Optimal errors and phase transitions in high-dimensional generalized linear models,” *Proceedings of the National Academy of Sciences* **116**, 5451–5460 (2019).
- [51] S. Goldt, M.S. Advani, A.M. Saxe, F. Krzakala, and L. Zdeborová, “Dynamics of stochastic gradient descent for two-layer neural networks in the teacher-student setup,” in *Advances in Neural Information Processing Systems 32* (2019).
- [52] Y. Yoshida, R. Karakida, M. Okada, and S.-I. Amari, “Statistical mechanical analysis of learning dynamics of two-layer perceptron with multiple output units,” *Journal of Physics A: Mathematical and Theoretical* **52** (2019).
- [53] R. Ge, J.D. Lee, and T. Ma, “Learning one-hidden-layer neural networks with landscape design,” in *ICLR* (2017) arXiv:1711.00501.
- [54] Y. Li and Y. Y., “Convergence analysis of two-layer neural networks with relu activation,” in *Advances in Neural Information Processing Systems* (2017) pp. 597–607.
- [55] S. Arora, N. Cohen, W. Hu, and Y. Luo, “Implicit Regularization in Deep Matrix Factorization,” in *Advances in Neural Information Processing Systems 33* (2019).
- [56] D.P. Kingma and M. Welling, “Auto-encoding variational bayes,” in *ICLR* (2014) arXiv:1312.6114.
- [57] D. Michelsanti and Z. Tan, “Conditional generative adversarial networks for speech enhancement and noise-robust speaker verification,” in *Proc. Interspeech 2017* (2017) pp. 2008–2012.
- [58] Q. Le, T. Szepesvári, and A. Smola, “Fastfood-approximating kernel expansions in loglinear time,” in *Proceedings of the international conference on machine learning*, Vol. 85 (2013).
- [59] M. Moczulski, M. Denil, J. Appleyard, and N. d. Freitas, “ACDC: A structured efficient linear layer,” in *International Conference on Learning Representations (ICLR)* (2016).
- [60] F.X. Yu, A.T. Suresh, K.M. Choromanski, D.N. Holtmann-Rice, and S. Kumar, “Orthogonal random features,” in *Advances in Neural Information Processing Systems* (2016) pp. 1975–1983.
- [61] D. Saad and S.A. Solla, “On-line learning in soft committee machines,” *Phys. Rev. E* **52**, 4225–4243 (1995).
- [62] D. Saad, *On-line learning in neural networks*, Vol. 17 (Cambridge University Press, 2009).
- [63] V.A. Marchenko and L.A. Pastur, “Distribution of eigenvalues for some sets of random matrices,” *Matematicheskii Sbornik* **114**, 507–536 (1967).
- [64] P. Riegler and M. Biehl, “On-line backpropagation in two-layered neural networks,” *Journal of Physics A: Mathematical and General* **28** (1995).
- [65] J. Hadamard, “Resolution d’une question relative aux déterminants,” *Bull. des sciences math.* **2**, 240–246 (1893).
- [66] D.E. Muller, “Application of boolean algebra to switching circuit design and to error detection,” *Transactions of the IRE professional group on electronic computers* **3**, 6–12 (1954).

- [67] I. S Reed, *A class of multiple-error-correcting codes and the decoding scheme*, Tech. Rep. (Massachusetts Inst of Tech Lexington Lincoln Lab, 1953).
- [68] D. Saad and S.A. Solla, "Learning with Noise and Regularizers Multilayer Neural Networks," in *Advances in Neural Information Processing Systems 9* (1997) pp. 260–266.
- [69] S. Mei, A. Montanari, and P. Nguyen, "A mean field view of the landscape of two-layer neural networks," *Proceedings of the National Academy of Sciences* **115**, E7665–E7671 (2018).
- [70] L. Chizat and F. Bach, "On the global convergence of gradient descent for over-parameterized models using optimal transport," in *Advances in Neural Information Processing Systems 31* (2018) pp. 3040–3050.
- [71] M. Biehl, P. Riegler, and C. Wöhler, "Transient dynamics of on-line learning in two-layered neural networks," *Journal of Physics A: Mathematical and General* **29** (1996).
- [72] M. Rattray, D. Saad, and S.-I. Amari, "Natural Gradient Descent for On-Line Learning," *Physical Review Letters* **81**, 5461–5464 (1998).
- [73] A.M. Saxe, J.L. McClelland, and S. Ganguli, "Exact solutions to the nonlinear dynamics of learning in deep linear neural networks," in *ICLR* (2014).
- [74] Y.N. Dauphin, R. Pascanu, G. Gulcehre, K. Cho, S. Ganguli, and Y. Bengio, "Identifying and attacking the saddle point problem in high-dimensional non-convex optimization," in *Advances in Neural Information Processing Systems* (2014) pp. 2933–2941.
- [75] D. Kalimeris, G. Kaplun, P. Nakkiran, B. Edelman, T. Yang, B. Barak, and H. Zhang, "Sgd on neural networks learns functions of increasing complexity," in *Advances in Neural Information Processing Systems 32* (2019) pp. 3496–3506.
- [76] V. Vapnik, "Statistical learning theory," New York, 156–160 (1998).
- [77] F. Farnia, J. Zhang, and D. Tse, "A spectral approach to generalization and optimization in neural networks," in *ICLR* (2018).
- [78] N. Rahaman, A. Baratin, D. Arpit, F. Draxler, M. Lin, F. A Hamprecht, Y. Bengio, and A. Courville, "On the spectral bias of neural networks," in *ICML* (2019).
- [79] D. Arpit, S. Jastrzębski, M.S. Kanwal, T. Maharaj, A. Fischer, A. Courville, and Y. Bengio, "A Closer Look at Memorization in Deep Networks," in *Proceedings of the 34th International Conference on Machine Learning* (2017).
- [80] C. Zhang, S. Bengio, M. Hardt, B. Recht, and O. Vinyals, "Understanding deep learning requires rethinking generalization," in *ICLR* (2017).
- [81] A.C.C. Coolen, D. Saad, and Y.-S. Xiong, "On-line learning from restricted training sets in multilayer neural networks," *EPL (Europhysics Letters)* **51**, 691 (2000).
- [82] A.C.C. Coolen and D. Saad, "Dynamics of learning with restricted training sets," *Physical Review E* **62**, 5444 (2000).
- [83] F. Gerace, B. Loureiro, F. Krzakala, M. Mézard, and L. Zdeborová, "Generalisation error in learning with random features and the hidden manifold model," (2020), arXiv:2002.09339.
- [84] F. Mignacco, F. Krzakala, Y. M. Lu, and L. Zdeborová, "The role of regularization in classification of high-dimensional noisy gaussian mixture," arXiv preprint arXiv:2002.11544 (2020).